International
Progress Report

IPR-02-47

Äspö Hard Rock Laboratory

TRUE-1 Continuation project

Complementary investigations at the TRUE-1 site - Crosshole interference, dilution and tracer tests, CX-1 - CX-5

Peter Andersson
Eva Wass
Sofia Gröhn
Magnus Holmqvist

GEOSIGMA AB

November 2002

Svensk Kärnbränslehantering AB
Swedish Nuclear Fuel
and Waste Management Co
Box 5864
SE-102 40 Stockholm Sweden
Tel +46 8 459 84 00
Fax +46 8 661 57 19

Äspö Hard Rock
Laboratory

Report no.
IPR-02-47
No.
F83K
Author
Peter Andersson
EvaWass
Sofia Gröhn
Magnus Holmqvist
Date
Nov 2002
Checked by
Anders Winberg
Date
Jan 2003
Approved
Christer Svemar
Date
03-04-17

Äspö Hard Rock Laboratory

TRUE-1 Continuation project

Complementary investigations at the TRUE-1 site - Crosshole interference, dilution and tracer tests, CX-1 - CX-5

Peter Andersson
Eva Wass
Sofia Gröhn
Magnus Holmqvist

GEOSIGMA AB

November 2002

Keywords: Complementary, cross-hole, dilution, fracture. interference, network, tracer

Abstract

Complementary investigations were performed at the TRUE-1 site as a part of the TRUE-1 Continuation Project. The investigations included three pressure interference tests combined with tracer dilution tests and two multiple-hole tracer tests using conservative tracers. The main objective of the tests was to obtain more information about the fracture network which the target structure, Feature A, is part of, and Feature A's relation to this network. The results of the tests confirm the hydrostructural model of the TRUE-1 site consisting of at least three well separated hydraulic units, Feature A, Feature B+D and Feature NW-2. This conclusion was also supported by a tracer test where no tracer transport between Features A and B could be detected. Hence, the flow regime may not be considered as three-dimensional in the scale of the tracer tests (up to 10 metres). The tracer tests also confirmed that the flow path used in earlier tracer tests (eg. STT-1 and STT-2) consists of two separate transport paths with similar transport properties.

Sammanfattning

Kompletterande undersökningar genomfördes på TRUE-1 siten som en del av TRUE-1 Continuation Project. Undersökningarna inkluderade tre interferenstester som kombinerades med utspädningsförsök och två spårförsök med icke-sorberande spårämnen som genomfördes med utnyttjande av ett flertal injiceringssektioner. Huvudsyftet med de genomförda försöken var att erhålla mer information om det spricknätverk, där den undersökta Feature A utgör en del, och hur Feature A är associerat med detta nätverk. Resultaten av försöken konfirmerar en hydrostrukturell modell av TRUE-1-siten där de huvudsakliga konduktiva enheterna utgörs av Feature A, Feature B+D och Feature NW-2. Denna slutsats understöddes också av resultaten av spårförsöken där ingen transport mellan Features A och B kunde noteras. Den aktuell flödesregimen kan därför inte betraktas som tredimensionell på en skala motsvarande de genomförda spårförsöken (mindre än 10 m). Spårförsöken konfirmerade också att en flödesväg som tidigare undersökts som en del av STT-1 och STT-2 försöken består av två separata flödesvägar med likartade transportegenskaper.

Executive summary

The first TRUE Stage was finalised during the year 2000 (Winberg et al., 2000). The results were presented and discussed during an international seminar in September 2000 (Svensk Kärnbränslehantering AB, 2001). The bottom line was that there exists ambiguity in the interpretation of transport/retention in the studied Feature A over the experimental time scales considered. It was identified that one available means to resort amongst the alternative interpretations (conceptual models) of transport/retention in the investigated feature is to carry out the epoxy resin injection and subsequent excavation and analyses as planned. During the seminar it was also identified that advantage should be taken of the instrumented borehole array at the TRUE-1 site to obtain more information about the fracture network which Feature A is part of, and Feature A's relation to this network.

The project TRUE-1 Continuation involves complementary investigations at the TRUE-1 site with the aim of exploring some of the unresolved issues from previous hydraulic and tracer tests performed at the site (Winberg et al., 2000).

The purposes of the TRUE-1 Continuation tests were to obtain more information about the internal structure of the target structure (Feature A), in particular the reason for the dual-peak breakthrough obtained during previously performed tracer tests and the relation between Feature A and the surrounding fracture network, in particular the interpreted Features B and NW-2.

The complementary investigations involved five different test set-ups, the three first (CX-1 to CX-3) involving tracer dilution tests combined with pumping and the two last (CX-4 and CX-5) including multiple-hole tracer tests.

The pumping and recovery phases of tests CX-1 to CX-3 were performed as conventional constant rate pressure interference tests implying that the flow rates and pressures were monitored with a high measurement frequency by the Äspö Hydro Monitoring System (HMS). Flow data from the sink section and the electrical conductivity of the withdrawal water were measured manually during the pumping period.

Tests CX-4 and CX-5 were focused on conservative tracer transport. CX-4 was performed with the aim to explore the cause of the double peak observed in the breakthrough curves obtained during the test STT-2 (Andersson et al., 1999a). The hypotheses being that the injection section KXTT4:R3 also included a water conducting splay fracture to Feature A (denoted A´) with similar water residence time. The two features were therefore separated by installing a short (0.5 m) extra packer making two sections, KXTT4:S2 and S3 of the former section R3.

Test CX-5 was performed with the purpose to assess connectivity between Feature B and A. Both tests were performed in a radially converging flow field with a constant withdrawal rate (controlled by a motorised valve and a mass flow meter) in borehole section KXTT3:R2 (Feature A). In CX-4 a pumping flow rate of Q=0.2 l/min (equivalent to that used during STT-2) was used and in CX-5 the pumping rate was Q=2.97 l/min. Injections were made according to Table 2-1, in two sections (Feature A and A´) in test CX-4 and in four sections (Feature A and B) in test CX-5. The tracers

(fluorescent dyes) were injected as decaying pulses and samples were continuously withdrawn both from the injection and withdrawal sections in accordance with earlier used techniques and equipment (Winberg et al., 2000).

In general, the performed tests confirm the existing hydro-structural model (Winberg et al., 2000. The pressure interference tests CX-1 and CX-3, using Feature A as sink, show similar response patterns, with high and fast responses in sections interpreted to include Feature A and fast but significantly lower responses in sections including the bounding fracture zone NW-2. Features B and D responds slower and show less response.

The large drawdown created during test CX-3 induces responses also in the bounding fracture zones NNW-4, NW-2 and NW-3, in particular in borehole KA3067A (Zones NW-2 and NW-3). There are only a few responses that do no follow the pattern described above, in particular the very good responses in sections KA30005A:R4, KA3005A:R5 and KXTT2:R1. These responses indicate that splay fractures t Feature A are present.

The re-instrumentation and subsequent testing of borehole KXTT4 where the section enclosing Feature A (section R3) was divided into two sections (S2 and S3) by means of a packer, clearly shows that section S2 includes a splay fracture to Feature A.

The determined flow rates using the tracer dilution method performed both under natural (ambient) gradient and during the pumping phase of tests CX-1 to CX-3 also confirm the hydro-structural model. Each test included dilution measurements of 12 sections and significant flow responses were noted as a consequence of all three tests and in almost all sections measured. The magnitude of flow and flow responses are governed by the local transmissivity of the borehole section and the hydraulic gradient. Thus, flow rates vary by three orders of magnitude (c.f. Tables 3-2 to 3-4).

Test CX-1 show significant responses in all but two sections (Table 3-2). Only three sections show increased flow while the rest show decreased flow rate. This is consistent with the prevailing hydraulic gradient where sections located at a “down gradient” position in relation to the pumping section are subject to a reversal or partial reversal of the flow direction whereas a section placed “up gradient” always shows an increase of flow. A similar pattern was noted during test CX-3 (Table 3-4) but due to the large drawdown, many of the sections show increased flow rates (7 out of 12).

Test CX-2 in Feature B generally show increased flow rates as the pumped section (KXTT4:S4) is located “down gradient” compared to Feature A.

The head distribution within Feature A is virtually unchanged since the 1996-1999 test period (TRUE-1). The hydraulic head has decreased about 4 metres since June 1997 but the head difference between the highest and lowest points over the 10 metre distance has decreased from about 1 m to about 0.6 m implying a somewhat lower hydraulic gradient (about 6%). The direction of the hydraulic gradient has changed somewhat to be more in the downward direction.

Feature B shows larger head differences and a similar direction of the natural gradient. The intercept in borehole KA3005A is clearly influenced by the closeness and possible intersection with Feature A which also is manifested during pumping in test CX-3 where the head difference between features A and B decreases to only 1.7 m.

The tracer test CX-4b was performed with the aim to explore the cause of the double peak observed in the breakthrough curves obtained during the test STT-2 (Andersson et al., 1999a). The test was performed by pumping in borehole section KXTT3:R2 (Feature A) with a rate of 0.2 l/min (same as in STT-2) resulted in breakthrough from both injection points located in Feature A, KXTT4:S2 and KXTT4:S3.

Results from modelling using a one-dimensional advection-dispersion model show significantly lower dispersivities for both individual flow paths than for the two flow paths combined, evaluated in STT-1 and RC-1 (D/v = 2 m). Mean travel times for the two flow paths (97 and 140 hours) are significantly longer than during STT-2 (8 and 26 hours) although the same strength of the sink was applied. The slower transport is possibly an effect of changed flow pattern or altered hydraulic characteristics for the flow path. The calculated hydraulic conductivity of the fracture is about one order of magnitude lower than that evaluated from the previously performed tests. This is also shown by the low injection flow rates which are about 20-100 times lower than in STT-2.

The tracer test CX-5 was performed with the purpose to assess connectivity between Features B and A. Test CX-5 was performed in a radially converging flow field with a constant withdrawal rate of Q=2.97 l/min in KXTT3:R2 (Feature A). Tracer injections were made in four sections, KXTT1:R2 and KXTT4:S3 in Feature A and KXTT1:R3 and KXTT4:S4 in Feature B. Tracer breakthrough was only detected from the two injections in Feature A, while no breakthrough could be detected from the two injections in Feature B over a time period of 700 hours, equivalent to about 30 days.

Results from modelling using a one-dimensional advection-dispersion model shows similar value of dispersivity for KXTT4:S3 as in CX-4b and somewhat lower dispersivity for the flow path KXTT1:R2 – KXTT3:R2 than previously evaluated (STT-1b), 0.2 m compared to 0.5 m. It is likely that the flow path is much narrower and less dispersed due to the extremely large gradient. This is also indicated by the lower values of equivalent fracture aperture and flow porosity than in previous runs.

The general conclusion that can be drawn from the combined results of the pressure interference tests, tracer dilution tests and tracer tests CX-1 – CX-5 is that the TRUE-1 array consists of at least three well separated hydraulic units, Feature A, Feature B+D and Feature NW-2. Hence, the flow regime may not be considered as three-dimensional in the scale of the tracer tests (up to 10 metres). In a larger scale it is obvious that the features are interconnected.

Contents

1 Introduction

1.1 Background

A programme has been defined to increase the understanding of the processes that govern retention of radionuclides transported in crystalline rock, the Tracer Retention Understanding Experiments (TRUE). The basic idea is to perform a series of tracer tests with progressively increasing complexity.

The First TRUE Stage was finalised during the year 2000 (Winberg et al., 2000). The results were presented and discussed during an international seminar in September 2000 (Svensk Kärnbränslehantering AB, 2001). The bottom line is that there exists ambiguity in the interpretation of transport/retention in the studied Feature A over the experimental time scales considered. It was identified that one available means to resort amongst the alternative interpretations (conceptual models) of transport/retention in the investigated feature is to carry out the epoxy resin injection and subsequent excavation and analyses as planned. However, due to the close proximity to the neighbouring LTDE (Long Term Diffusion Experiment) site, the fact that the two sites are hydraulically conducted, and the LTDE project (Byegård et al., 1999) having a high priority implies that the planned resin injection will be postponed in time at least till 2004.

During the seminar it was also identified that the advantage should be taken of the instrumented borehole array at the TRUE-1 site to obtain more information about the fracture network which Feature A is part of, and Feature A's relation to this network.

The new project, TRUE-1 Continuation, involves complementary investigations at the TRUE-1 site with the aim of exploring some of the unresolved issues from previous hydraulic and tracer tests performed at the site (Winberg et al., 2000).

Before initiating the tests described in this report, a pre-study was performed aiming at describing the history and current situation of inflow to the tunnel, water pressure, water chemistry and status of the borehole instrumentation at the TRUE-1 site (Källgården et al., in prep.)

1.2 Objectives

The purposes of the TRUE-1 Continuation tests were in particular to obtain more information about the internal structure of the target structure (Feature A) and the relation between Feature A and the surrounding fracture network, in particular the interpreted Features B and NW-2. Specific objectives with the tests were to:

- verify the hydro-structural model of the TRUE-1 site by means of pressure interference tests in combination with the tracer dilution tests. Such tests have not been performed within the current borehole instrumentation and after drilling of borehole KXTT5.
- investigate the reasons for the "double-peak" breakthrough observed during tracer test STT-2 (Andersson et al., 1999). The hypothesis was that two separated flow paths exists between the borehole sections used for injection and withdrawal during STT-2, KXTT4:R3 and KXTT3:R2 (c.f. Winberg et al., 2000).
- establish whether or not any fast interconnecting flow path exists between features A and B.

2 Performance and evaluation procedure

2.1 Equipment and tracers used

Each borehole in the TRUE -1 array is instrumented with 4-5 inflatable packers such that 4-5 borehole sections are isolated. All isolated borehole sections are connected to the HMS-system through data loggers (Datascan). The sections planned to be used for tracer tests are equipped with three nylon hoses, two with an inner diameter of 4 mm and one with an inner diameter of 2 mm. The two 4-mm hoses are used for injection, sampling and circulation in the borehole section whereas the 2-mm hose is used for pressure monitoring.

The tracer dilution tests were performed using four identical equipment set-ups for tracer tests, i.e. allowing four sections to be measured simultaneously. A schematic drawing of the tracer test equipment is shown in Figure 2-1. The basic idea is to have an internal circulation in the borehole section. The circulation makes it possible to obtain a homogeneous tracer concentration in the borehole section and to sample the tracer concentration outside the borehole in order to monitor the injection rate of the tracer with time, and also the dilution rate.

Circulation is controlled by a pump with variable speed (A) and measured by a flow meter (B). Water and tracer injections are made with two different HPLC plunger pumps (C1 and C2) and sampling is made by continuously extracting a small volume of water from the system through a flow controller (constant leak) to a fractional sampler (D). Water and tracer solution is stored in two separate pressurised vessels (E1 and E2) under nitrogen atmosphere. The tracer test equipment has earlier been used in the TRUE-1 tracer tests (e.g. Andersson, 1996).

The tracers used were three fluorescent dye tracers, Uranine (Sodium Fluorescein) from KEBO (purum quality), Amino G Acid from Aldrich (techn.quality) and Rhodamine WT from Holiday Dyes Inc. (techn. quality). These tracers have all been used extensively in the TRUE-1 tracer tests and in the TRUE Block Scale tracer tests (Andersson et al., 2002).

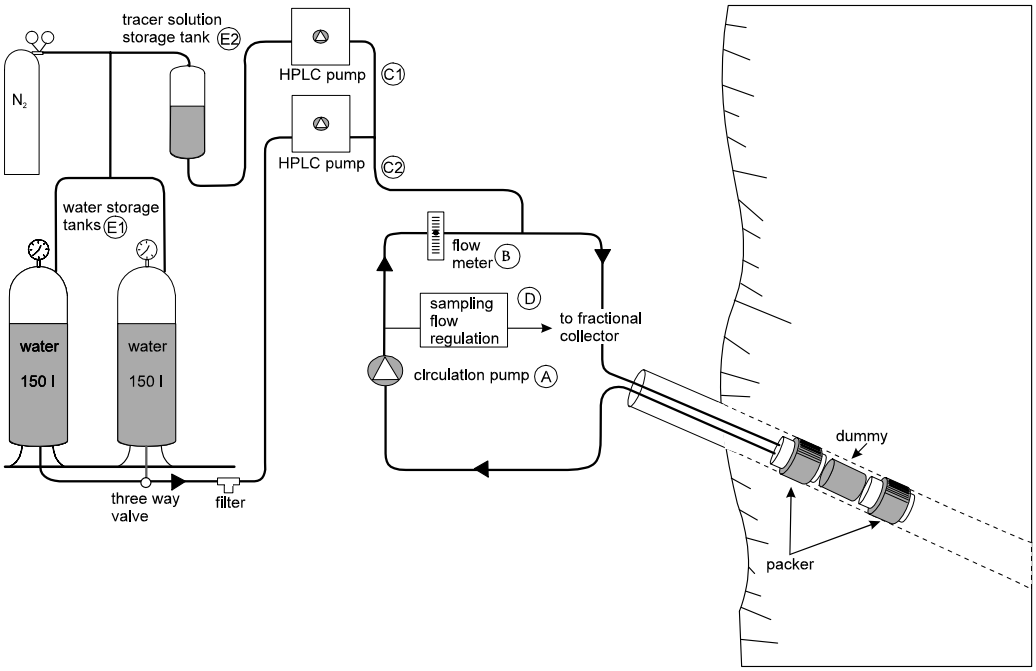

Figure 2-1 *Schematic drawing of the tracer injection/sampling system used in the TRUE Project.*

2.2 Performance of the dilution tests, interference tests and tracer tests, CX-1 - CX-5

The TRUE-1 Continuation complementary investigations involved five different test set-ups, the three first (CX-1 to CX-3) with tracer dilution tests combined with pumping and the two last (CX-4 and CX-5) including multiple-hole tracer tests.

The test cycle for tests CX-1 to CX-3 was similar to the one used in the TRUE Block Scale pre-tests PT-1 to PT-4 (Andersson et al., 1999b) and in the Phase A tests (Andersson et al., 2000). Each test (CX-1 - CX-3) included measurements in 12 borehole sections and had a test cycle of five days with a pumping period of 48 hours. The following test cycle was used:

Day 1 (pm) - start tracer dilution test under natural gradient in sections 1-4

Day 2 (am) - change of test sections to four new locations (sections 5-8)

Day 2 (pm) - start pumping in selected sink section

Day 3 (am) - change of test section to the four first tested (sections 1-4)

Day 3 (pm) or Day 4 (am) – change of test section to sections 9-12

Day 4 (pm) – stop pumping

Day 5 (am) – stop measurement in sections 9-12.

The withdrawal flow was established using the maximum sustainable flow rate. The dimension of the tubing and the hydraulic transmissivity of the section then only restricted the flow.

The pumping and recovery phases were performed as conventional constant rate pressure interference tests, implying that the flow rates and pressures were monitored with a high measurement frequency by the Äspö Hydro Monitoring System (HMS). Flow data from the sink section and the electrical conductivity of the withdrawal water were measured manually during the pumping period.

Tests CX-4 and CX-5 were focused on tracer transport. CX-4 was performed with the aim to explore the cause of the double peak observed in the breakthrough curves obtained during the test STT-2 (Andersson et al., 1999a). The hypothesis being that the injection section KXTT4:R3 also included a water conducting splay fracture to Feature A (denoted A´) with similar transport properties. The two features were therefore separated by installing a short (0.5 m) extra packer making two sections, KXTT4:S2 and S3 of the former section R3. In CX-4 a radially converging flow field with a constant withdrawal rate of Q=0.2 l/min (equivalent to that used during STT-2) was used (controlled by a motorised valve and a mass flow meter) in borehole section KXTT3:R2 (Feature A). Tracer injections were made according to Table 2-1, in two sections (Feature A and A´). The tracers (fluorescent dyes) were injected as decaying pulses and samples were continuously withdrawn both from the injection and withdrawal sections in accordance with earlier used techniques and equipment (Winberg et al., 2000)

Test CX-5 was performed with the purpose to assess connectivity between Feature B and A. The same sink (KXTT3:R2) was used but the pumping rate was Q=2.97 l/min. and tracer injections were made in four sections in both features, cf. Table 2-1. Tracers and sampling procedures were similar to test CX-4.

Table 2-1 summarises the test set-ups including the sources and sinks used in the tests. Locations of the boreholes in the TRUE-1 array are shown in Figure 2-2 together with the main fractures in the rock volume.

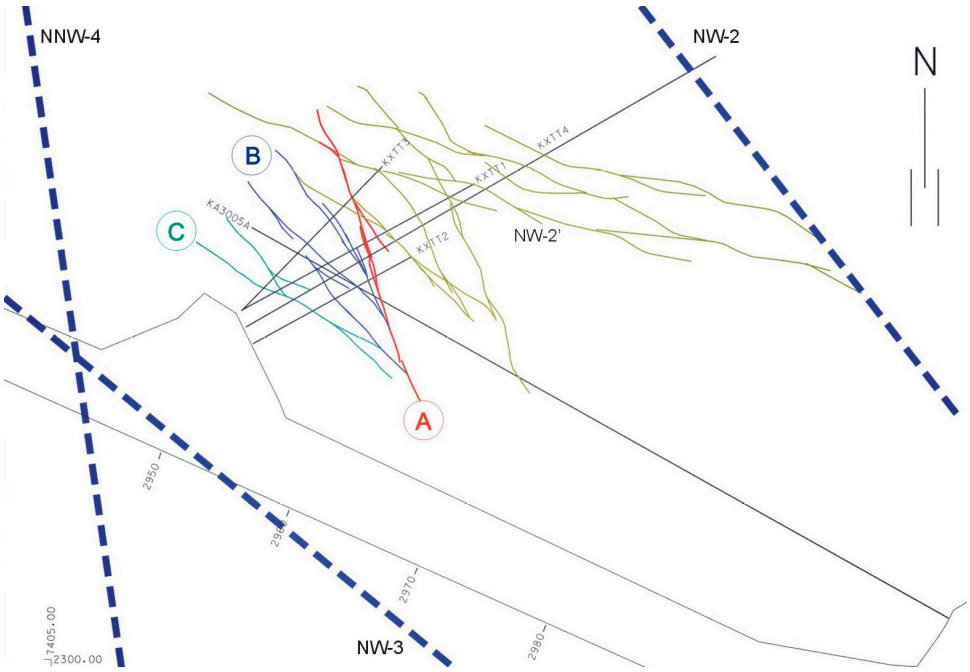

Figure 2-2 *Horizontal section at Z=–400 masl showing structural model based on identified conductive geological structures in the TRUE-1 rock volume. Also, 5 of 6 boreholes in the TRUE-1 array are seen (KXTT5 missing).*

Table 2-1. Sources and sinks used for the complementary tests at the TRUE-1 site. Section limits and borehole diameters for all boreholes at the TRUE-1 site are given in Appendix 1

Test	Sink	Feature	Source	Feature	Comment
CX-1	KXTT4:S3	A	KXTT1:R2	A	Tracer dilution/interference test
CX-2	KXTT4:S4	B	KXTT1:R3	B	Tracer dilution/interference test
CX-3	KXTT3:R2	A	KXTT2:R2	A	Tracer dilution/interference test
			KXTT2:R3	B	
			KXTT3:R2	A	Only test CX-1 and CX-2
			KXTT3:R3	B	
			KXTT4:S2	A´	
			KXTT4:S3	A	Only test CX-2 and CX-3
			KXTT4:S4	B	Only test CX-1 and CX-3
			KXTT5:P2	A	
			KA3005A:R2	B	
			KA3005A:R3	A	
			KA3010A:P2	NW-2	
CX-4	KXTT3:R2	A	KXTT4:S2	A´	Tracer test (radially converging)
			KXTT4:S3	A	
CX-5	KXTT3:R2		KXTT4:S4	B	Tracer test (radially converging)
			KXTT1:R3	B	
			KXTT4:S3	A	
			KXTT1:R2	A	

2.3 Laboratory analyses

Samples were analysed for dye tracer content at the SKB BASLAB Laboratory using a TD-700 Digital Laboratory Fluorometer /Turner Designs.

2.4 Evaluation

2.4.1 Hydraulic interference tests

The evaluation involves preparation of pressure response diagrams for each test and a common pressure response matrix for all tests.

Time-drawdown (and recovery) plots were prepared for borehole sections showing a total drawdown of more than s_p=0.1 m (1 kPa) at stop of the flow period. This threshold pressure was chosen with consideration of the amplitude of the tidal effects in the boreholes which may be in the order of 1-5 kPa. From these plots, the response times (t_R) for each section were estimated. The response time is here defined as the time after start of pumping when a drawdown (or recovery) of 1 kPa is observed (from the logarithmic plots) in the observation section. The qualitative evaluation has mainly been made on data from the drawdown phase. Data from the recovery phase were used only as supporting data.

On the X-axis of the pressure response diagrams (Figures 3-2, 3-5 and 3-8), the ratio of the response time (t_R) and the (squared) straight-line distance R between the (midpoint of) the sink section and (the midpoint of) each observation section (t_R/R^2) is plotted. The latter ratio is inversely related to the hydraulic diffusivity of the rock, which indicates the speed of propagation in the rock of the drawdown created in the pumping section.

The final drawdown at stop of pumping (s_p) in the observation sections was determined from the drawdown data. To account for the different flow rates used in the tests and to make the pressure response plots comparable between tests, the final drawdown is normalised with respect to the final flow rate (Q_2). The ratio s_p/Q_2 is plotted on the Y-axis of the pressure response diagrams.

From the response plots of s_p/Q_2 versus t_R/R^2 for each test, sections with anomalous, fast response times (high hydraulic diffusivity) and large (normalised) drawdown can be identified. Such sections, showing primary responses, can be assumed to have a distinct hydraulic connection to the sink section and may be intersected by a single fracture; fracture zones or other conductive structures in the rock. On the other hand, sections with delayed and weak (secondary) responses may correspond to sections in the rock mass between such structures.

From the calculated values of s_p/Q_2 (index 1) and t_R/R^2 (index 2) for each observation section during each test, a common pressure response matrix showing the response patterns for all tests, was prepared by classifying the pressure responses by means of the above indexes 1 and 2. For index 1, the following class limits and associated drawdown characteristics were used:

Index 1 (s_p/Q_2)

$s_p/Q_2 > 1 \cdot 10^5$ s/m^2	Excellent (Red)
$3 \cdot 10^4 < s_p/Q_2 \leq 1 \cdot 10^5$ s /m^2	High (Yellow)
$1 \cdot 10^4 < s_p/Q_2 \leq 3 \cdot 10^4$ s /m^2	Medium (Green)
$s_p/Q_2 \leq 1 \cdot 10^4$ s /m^2	Low (Blue)

For index 2 the following class limits and associated response characteristics were used:

Index 2 (t_R/R^2)

$t_R/R^2 < 0.01$ s/m^2	Excellent (E)
$0.01 \leq t_R/R^2 < 0.1$ s/m^2	Good (G)
$0.1 \leq t_R/R^2 < 0.3$ s/m^2	Medium (M)
$t_R/R^2 \geq 0.3$ s/m^2	Bad (B)

The results from the qualitative analysis of the hydraulic responses were compared with the hydro-structural model and the latter checked for consistency and possible need of revision. It should be pointed out that the response diagrams of s_p/Q_2 versus t_R/R^2 described above were only used as diagnostic tools to identify the most significant responses during each test and to construct the pressure response matrix. The diagrams should be used with some care since the true actual distances (along pathways) between the sink and observation sections are uncertain, which may affect the position of a certain point (i.e. section) in the horizontal direction in the diagrams. However, in most cases, the shortest (straight-line) distance between the sink and observation section, as used here, is considered as a sufficient and robust approximation for the above purpose.

Another potential source of error in the response diagrams may occur if (internal) hydraulic interaction exists between sections along an observation borehole. For example, such interaction could either be due to packer leakage (insufficient packer sealing) or leakage in the rock through interconnected fractures around the packers. This fact may give rise to a false impression that good hydraulic communication exists between such observation sections and the actual source section. However, any analysis method will suffer from this potential source of error.

2.4.2 Tracer dilution tests

Flow rates were calculated from the decay of tracer concentration versus time through dilution with natural unlabelled groundwater, c.f. Winberg (*ed*), (1996). The so-called "dilution curves" were plotted as the natural logarithm of concentration versus time. Theoretically, a straight-line relationship exists between the natural logarithm of the relative tracer concentration (c/c_0) and time (t):

$$Q_{bh} = -V \cdot \Delta \ln (c/c_0) / \Delta t \qquad 2\text{-}1$$

where Q_{bh} (m^3/s) is the groundwater flow rate through the borehole section and V (m^3) is the volume of the borehole section.

2.4.3 Tracer tests

The evaluation of the tracer test has involved computer modelling using a simple one-dimensional advection-dispersion model (Van Genuchten & Alves, 1982). From the computer modelling, dispersivity and mean travel times were determined using an automated parameter estimation program, PAREST (Nordqvist, 1994). PAREST uses a non-linear least square regression where regression statistics (correlation, standard errors and correlation between parameters) also is obtained.

The chosen one-dimensional model assumes a constant fluid velocity and negligible transverse dispersion, cf. Equation 2-2.

$$\partial C/\partial t = D(\partial^2 C/\partial x^2) - v \cdot \partial C/\partial x \qquad 2\text{-}2$$

where: D = Dispersion coefficient

v = fluid velocity (m/s)

C = concentration of solute

x = distance from injection point (m)

t = time (s)

According to Ogata & Banks (1961) and Zuber (1974), the dispersion in a radially converging flow field can be calculated with good approximation by equations valid for one-dimensional flow. Although a linear flow model (constant velocity) is used for a converging flow field, it can be demonstrated that breakthrough curves and parameter estimates are similar for Peclet numbers of about 10 and higher.

Van Genuchten (1982) gives a solution for step input with dispersion over the injection boundary. The solution of Equation 2-2 then is:

$$C/C_o = \tfrac{1}{2}\,\mathrm{erfc}\,[(x-v\cdot t)/Z] + (V/\pi)^{1/2} \exp\,[(x-v\cdot t)^2/(4D\cdot t)] - \qquad 2\text{-}3$$

$$\tfrac{1}{2}\,[1+v\cdot x/D+V]\,\exp\,[v\cdot x/D]\,\mathrm{erfc}[(x+v\cdot t)/Z]$$

where: $Z = 2(D\cdot t)^{1/2}$

$V = v^2 t/D$

Variable injection schemes were simulated by superposition of the solution given in Equation 2-3.

The fit of the breakthrough curves using a three-parameter fit included velocity, v, dispersion coefficient, D, and the so called F-factor which corresponds to injected mass divided by fracture volume, M_{inj}/V_f. The result of the evaluation is presented in Chapter 3.6.3 and 3.7.3.

Based on the mean travel times, t_m, determined from the parameter estimation, the hydraulic fracture conductivity, K_{fr} (m/s), were calculated assuming radial flow and validity of Darcy's law (Gustafsson & Klockars, 1981);

$$K_{fr} = \ln (r/r_w) (r^2 - r_w^2) / 2 \cdot t_m \cdot \Delta h \qquad 2\text{-}4$$

where: r = travel distance (m)

r_w = borehole radius (m)

t_m = mean travel time of tracer (s)

Δh = head difference (m)

The equivalent fracture aperture, b (m), was calculated from:

$$b = Q \cdot t_m / \pi \cdot (r^2 - r_w^2) \qquad 2\text{-}5$$

where Q (m^3/s), is the mean pumping rate.

Flow porosity, θ_k, was calculated using:

$$\theta_k = K/K_{fr} \qquad 2\text{-}6$$

where K is the hydraulic conductivity of the packed-off section of the borehole determined from steady state evaluation of the interference test (Moye, 1967):

$$K = (Q/\Delta h \cdot L) \cdot ((1+\ln L/2r_w)/2\pi) \qquad 2\text{-}7$$

where L (m) is the length of the packed-off section. It should be noted that the term flow porosity might be misleading to use in a fractured heterogeneous rock as it is defined for a porous media. However, it is often used in fractured media as a scaling factor for transport, but then defined over a finite thickness which, in his case, is defined as the length of the packed-off borehole section (L = 2.0 m).

The values calculated using Equations 2-4 through 2-7 are presented together with parameters determined from the numerical modelling of the tracer breakthrough in Table 3-11.

Tracer mass recovery was calculated for all flow paths/tracers used. The tracer mass recovered in the pumping borehole section was determined by integration of the breakthrough curves for mass flux (mg/h) versus time (h). The injected mass was calculated by weighing the tracer solution vessel during the injection procedure.

3 Results and interpretation

3.1 General

The equipment has worked well and no major hydraulic disturbance occurred during the tests except a packer failure in KXTT5 during test CX-5. This failure caused a minor change in the hydraulic gradient during the test, cf. Chapter 3.8. A Log of events during the tests is presented in Table 3-1.

Table 3-1. Log of events

Date	Event
020121	Start tracer dilution tests **CX-1**
020122	Start pumping KXTT4:S3, Q=0.57 l/min
020125	Stop pumping KXTT4:S3
020128	Stop tracer dilution tests **CX-1**, Start tracer dilution tests **CX-2**
020129	Start pumping KXTT4:S4, Q=0.53 l/min
020201	Stop pumping KXTT4:S4
020204	Stop tracer dilution tests **CX-2**, Start tracer dilution tests **CX-3**
020205	Start pumping KXTT3:R2, Q=2.64 l/min
020207	Stop pumping KXTT3:R2
020208	Stop tracer dilution tests **CX-3**
	Test CX-4
020208	Start pumping KXTT3:R2, Q=0.2 l/min
020212	Tracer injection in KXTT4:S2 (Uranine) and KXTT4:S3 (Amino-G acid), CX-4a
020312	Tracer injection in KXTT4:S2 (Uranine) and KXTT4:S3 (Rhodamine WT), CX-4b
020318	Opening of borehole KA3065A03 (pressure disturbance)
020402	Closing of borehole KA3065A03
020403	Stop sampling CX-4
020406	Stop pumping KXTT3:R2, power failure
	Test CX-5
020409	Start pumping KXTT3:R2, Q=2.97 l/min
020416	Tracer injection in KXTT1:R2 (Uranine), KXTT4:S3 (Amino-G acid) and KXTT4:S4 (Rhodamine WT)
020417	Tracer injection in KXTT1:R3 (Uranine)
020423	Packer failure in KXTT5
020506	Packers in KXTT5 reinflated
020514	Stop sampling CX-5
020514	Stop pumping KXTT3:R2

3.2 Pressure response matrix

The pressure response matrix for tests CX-1 to CX-3 is shown in Figure 3-1. The matrix is based on the pressure response diagrams for each test. The colours and letters coding refers to the two indexes s_p/Q (drawdown normalised to pumping rate) and t_R/R^2 (response time normalised to the distance squared) according to Chapter 2.4.1.

Figure 3-1 shows that the pressure response pattern during test CX-1 and CX-3, both with sink in Feature A, are very similar. These tests generally show high and fast responses in sections interpreted to include Feature A. In test CX-2, with the sink in Feature B, most sections responding fast and high are interpreted to include Feature B, and in some cases also Feature D. The results of each test are discussed in more detail below.

Sink in Feature		A	B	A	
Borehole	Interval (m)	CX-1	CX-2	CX-3	Structure
KXTT1:R1	17.00-28.76	B	B	M	NW-2´
KXTT1:R2	15.00-16.00	E	B	G	A
KXTT1:R3	7.50-11.50	B	G	M	B
KXTT1:R4	3.00-6.50	B	G	B	D
KXTT2:R1	16.55-18.30	B	M	M	?
KXTT2:R2	14.55-15.55	M	M	M	A
KXTT2:R3	11.55-13.55	B	M	B	B
KXTT2:R4	7.55-10.55	B	B	M	B
KXTT2:R5	3.05-6.55	G	M	G	D
KXTT3:R1	15.42-17.43	M	B	B	NW-2´
KXTT3:R2	12.42-14.42	M	B	S	A
KXTT3:R3	8.92-11.42	B	G	B	B
KXTT3:R4	3.17-7.92	B	G	B	B+D
KXTT4:S1	14.92-49.31	B	B	G	NW-2
KXTT4:S2	12.92-13.92	B	G	B	A´
KXTT4:S3	11.92-12.42	S	G	B	A
KXTT4:S4	8.42-10.92	B	S	M	B
KXTT4:S5	3.17-7.42	B	G	M	B+D
KXTT5:P1	10.81-25.85	B	B	M	NW-2
KXTT5:P2	9.61-9.81	G	M	M	A
KXTT5:P3	6.11-8.61	B	M	B	B
KXTT5:P4	3.11-5.11	B	M	B	D
KA3005A:R2	46.78-50.03	B	B	M	B
KA3005A:R3	44.78-45.78	G	B	G	A
KA3005A:R4	39.03-43.78	M	B	M	A?
KA3005A:R5	6.53-38.03	B	B	G	?
KA3010A:P2	8.56-15.06			B	NW-2
KA3067A:1	34.55-40.05			M	?
KA3067A:2	30.55-33.55			M	?
KA3067A:3	28.05-29.55			G	NW-2?
KA3067A:4	6.55-27.05			M	NW-3
KA3105A:P1	53.01-68.95			B	
KA3105A:P2	25.51-52.01			B	
KA3105A:P3	22.51-24.51			B	
KA3105A:P4	17.01-19.51			B	
KA3110A:P1	20.05-28.63			B	NNW-4
KA3110A:P2	6.55-19.05			B	
KA2050A:P1	155-211.57			M	
KA2050A:P2	102-154			M	NW-2?
KA2050A:P3	6-101			B	
KA2862A:P1	7.37-15.98			B	NW-3
HA1960A:P1	4-32			B	NNW-4

INDEX 1=Sp/Q
EXCELLENT
HIGH
MEDIUM
LOW

INDEX 2=tR/R2
E=EXCELLENT
G=GOOD
M=MEDIUM
B=BAD

S=SINK

Figure 3-1. *Pressure response matrix for TRUE-1 Continuation tests CX-1 through CX-3.*

3.3 Test CX-1

The first test, CX-1, performed by pumping borehole section KXTT4:S3 (Feature A), shows pressure responses (>1 kPa) in all 25 borehole sections within the TRUE-1 array over distances ranging between 1 and 27 m.

The response pattern (Figure 3-2) generally confirms the hydro-structural model with high and fast responses in sections interpreted to include Feature A. The magnitude of the hydraulic responses in Feature A is typically between 20-100kPa while responses in other section/features are less than 10 kPa. However, there are some responses that do not follow this pattern, in particular the very good responses in KA3005A:R4 and R5 indicating that these may be splay fractures to Feature A in section KA3005A:R3. This confirms earlier standpoint in Winberg et al (2000). The relatively good response in section KXTT2:R1 may also result from a water conducting splay fracture located at 17.20 m borehole length. This fracture has a similar orientation as the splay fracture (A´) in KXTT4:S2 and may in fact be the same. The responses in sections interpreted to include Feature NW-2 also respond in a similar way and significantly faster than Features B and D (Figure 3.2).

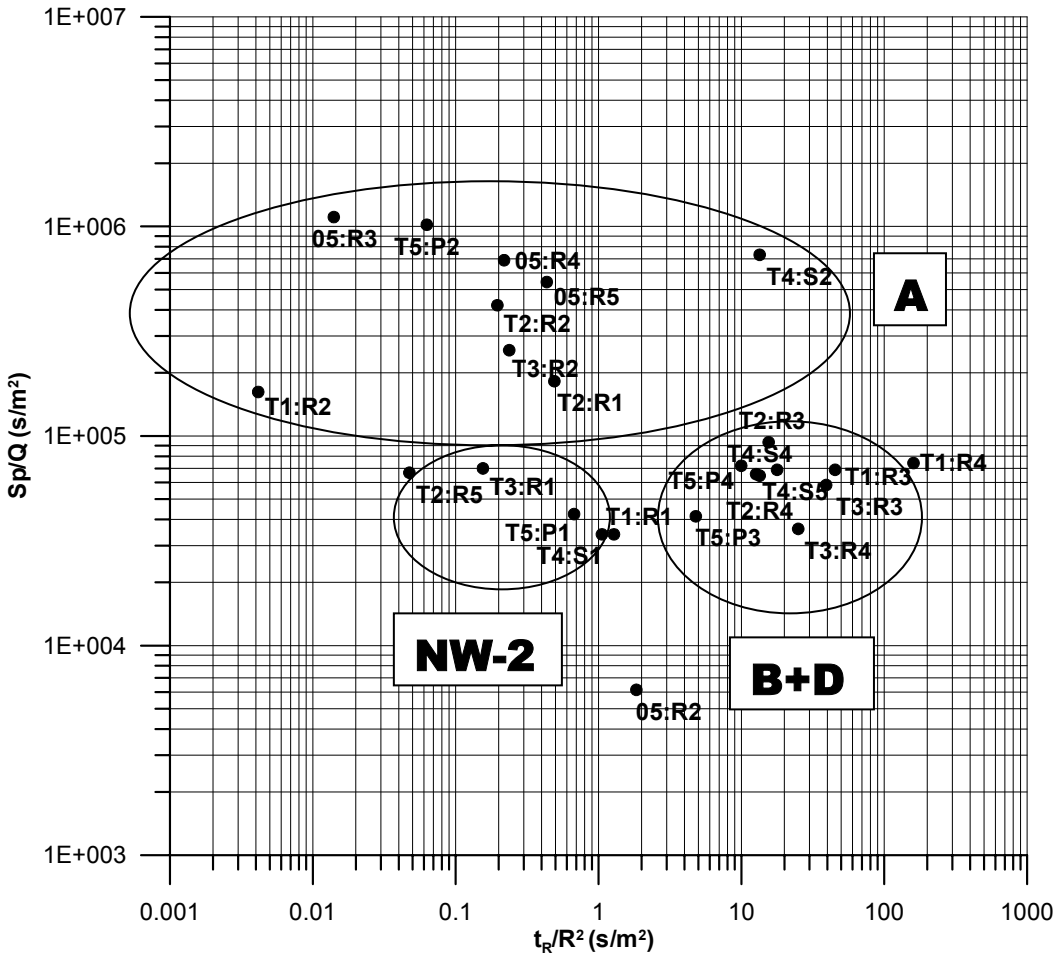

Figure 3-2. *Diagnostic plot of pressure responses during test CX-1. The encircled areas mark the responses of different Features. Borehole notations are shortened by removing the prefix "KXT-" and"KA30-" from the borehole labels, cf. Table 2-1.*

The pump rate and the electrical conductivity versus time are shown in Figure 3-3. The pumping flow rate decreased from 0.58 l/min to about 0.56 l/min during the pumping period. An increase in the electrical conductivity from 915 to 955 mS/m indicating an increasing portion of saline water was also noted.

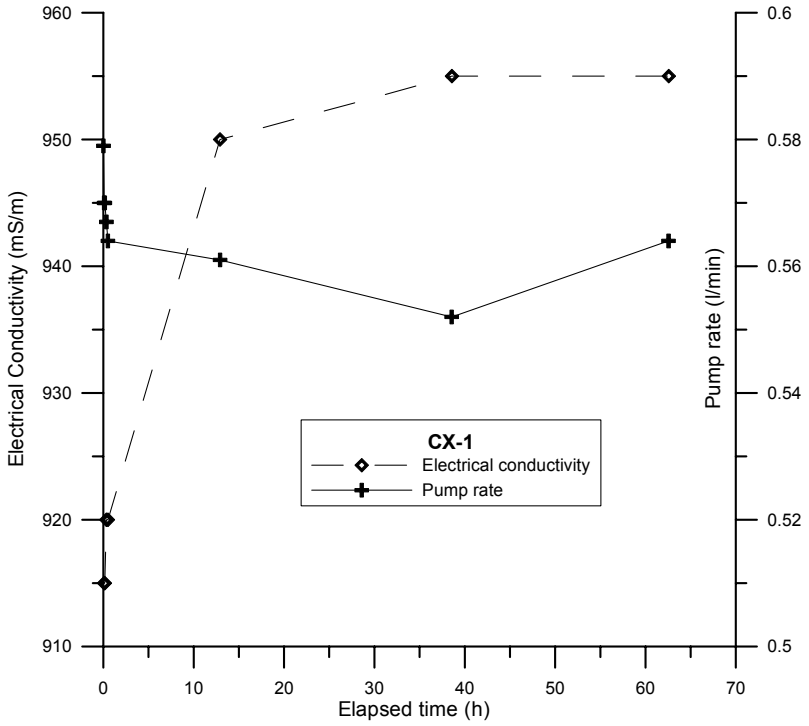

Figure 3-3. *Pump rate and electrical conductivity of the pumped water from KXTT4:S3 during test CX-1.*

Test CX-1 also included measurements of flow rates using the tracer dilution method in twelve selected observation sections. The measurements were performed both under natural gradient and during pumping of section KXTT4:S3 (Feature A) in order to study the influence of the pumping. The results presented in Table 3-2 show a distinct influence in many of the tested sections.

The most striking result is that the flow direction is changed in many cases as indicated by a decrease in the flow rate, cf. Figure 3-4. The only sections where a clear increase in the flow is registered are in sections KXTT3:R2 and KXTT5:P2, both including Feature A. The other sections in Feature A and Feature B show a decrease in the flow rate. This is consistent with the direction of the hydraulic gradient which is towards the tunnel, cf. Figure 4-2.

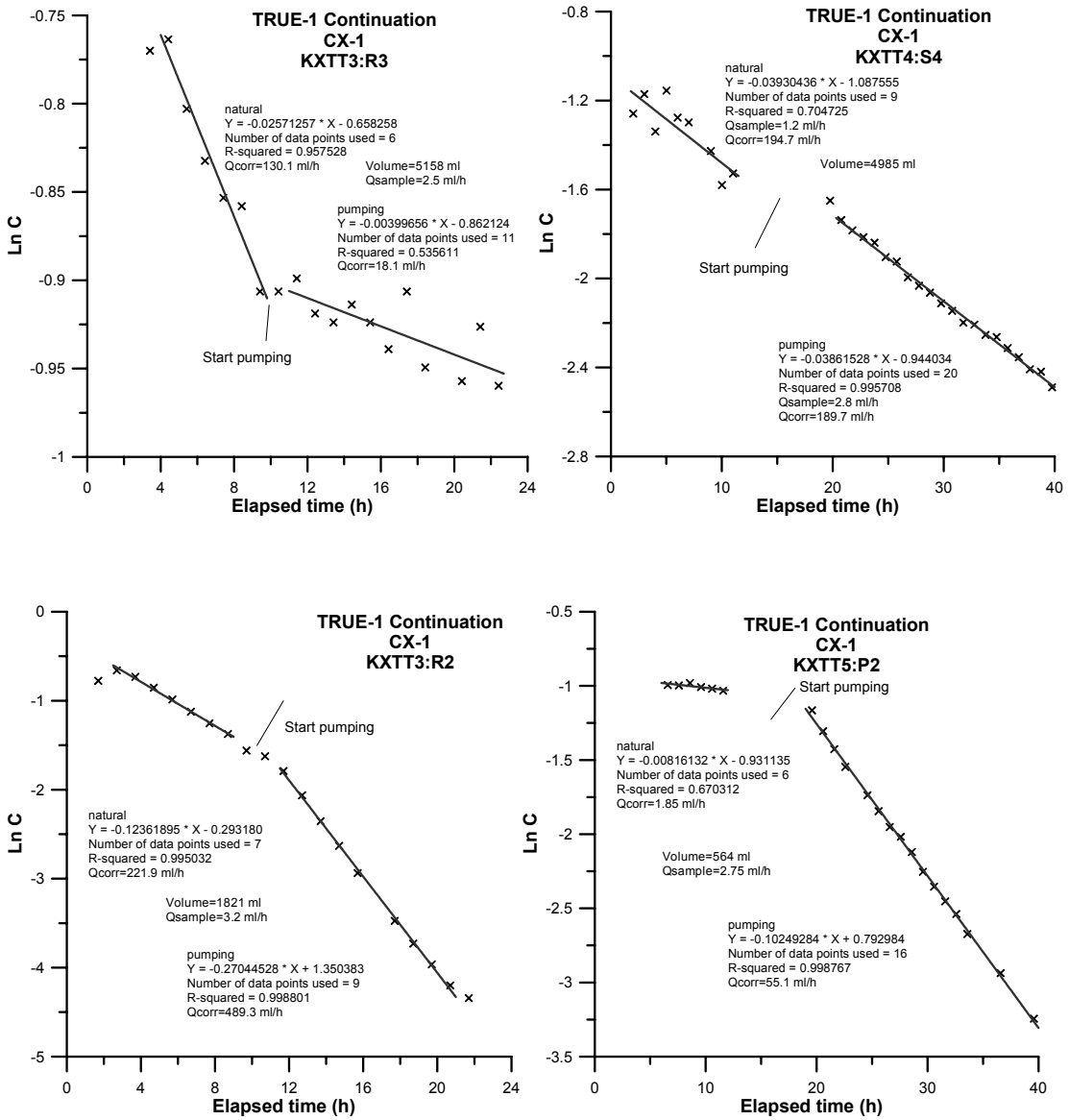

Figure 3-4. *Examples of tracer dilution graphs (Logarithm of concentration versus time) for sections KXTT3:R3 (Feature B), KXTT4:S4 (Feature B), KXTT3:R2 (Feature A) and KXTT5:P2 (Feature A), test CX-1. Steeper dip of the straight-line fit implies a higher flow rate.*

Table 3-2. Results of tracer dilution tests during test CX-1 using KXTT4:S3 (Feature A) as sink.

Test section	Feature	Section volume (ml)	$Q_{natural}$ (ml/h)	Q_{pump} (ml/h)	ΔQ (ml/h)
KXTT1:R2	A	1466	2	9	+7
KXTT1:R3	B	8181	122	107	-15
KXTT2:R2	A	1455	16	7	-9
KXTT2:R3	B	4205	31	13	-18
KXTT3:R2	A	1821	222	489	+267
KXTT3:R3	B	5158	130	18	-112
KXTT4:S2	A’	1414	7	4	-3
KXTT4:S3	A	1156		SINK	
KXTT4:S4	B	4985	195	190	-5
KXTT5:P2	A	564	2	55	+53
KA3005A:R2	B	7852	?	19	?
KA3005A:R3	A	2192	10	4	-6
KA3010A:P2	NW-2	13742	831	828	-3

3.4 Test CX-2

Test CX-2, performed by pumping borehole section KXTT4:S4 (Feature B), shows pressure responses (>1 kPa) in all 25 borehole sections within the TRUE-1 array over distances ranging between 2 and 28 m.

The response pattern during this test also generally confirms the hydro-structural model. Most of the sections responding fast and good (in the upper left corner of Figure 3-5) are interpreted as being associated with Feature B and also Feature D. Features A and NW-2 responds less well. The magnitude of the hydraulic responses in Features B and D are typically between 100-500 kPa whereas responses in Features A and NW-2 are less than 10kPa.

The pumping flow rate decreased from 0.76 l/min to about 0.44 l/min during the pumping period. The electrical conductivity was almost constant, 940 mS/m, cf. Figure 3-6.

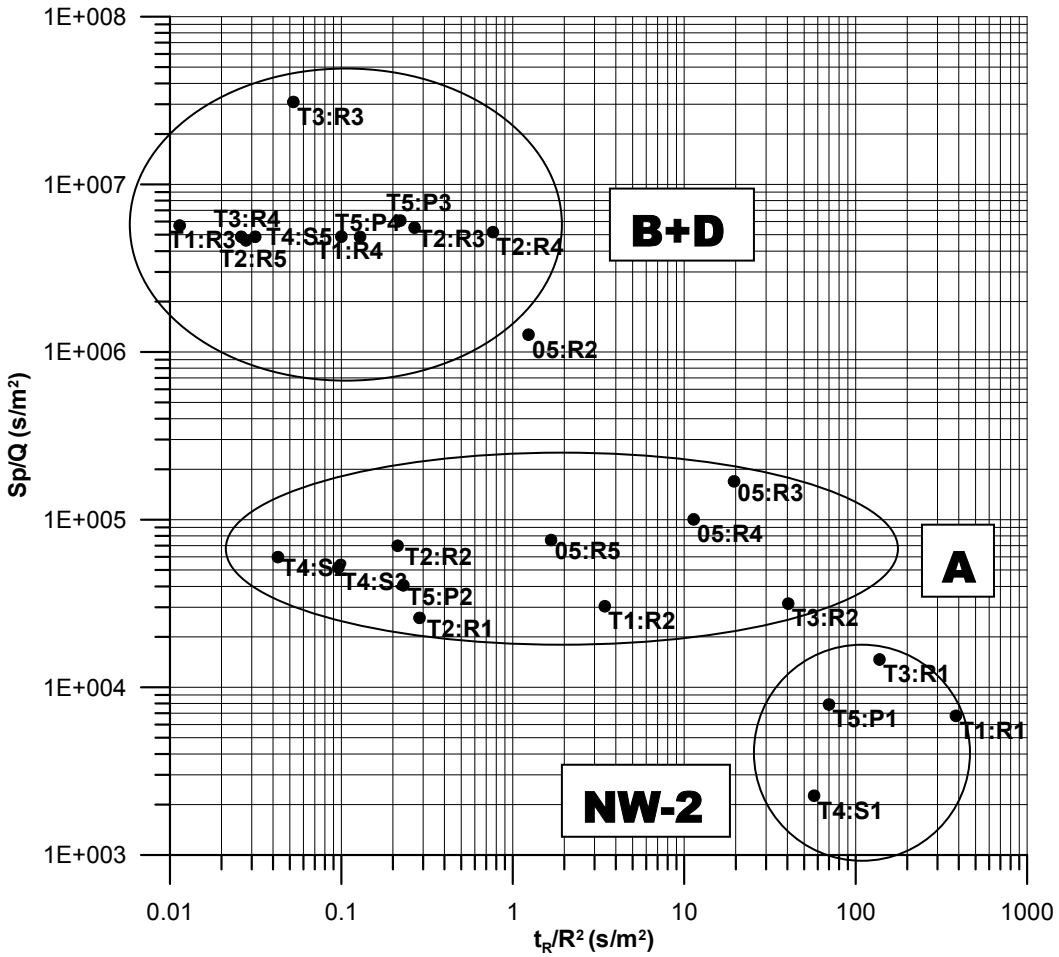

Figure 3-5. *Diagnostic plot of pressure responses during test CX-2. The encircled areas marks the the responses of different Features. Borehole notations are shortened by removing the prefix "KXT-" and"KA30-" from the borehole labels, cf. Table 2-1.*

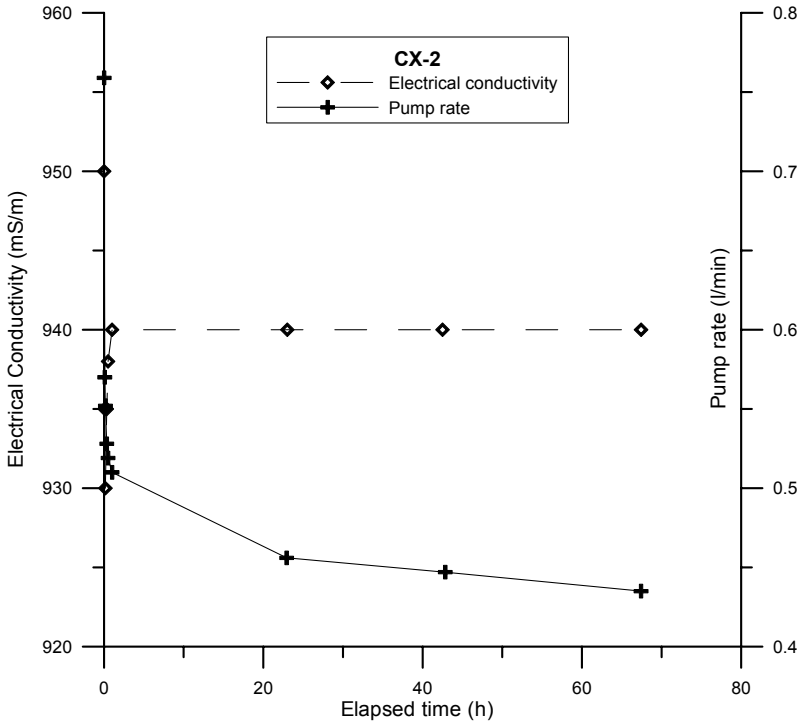

Figure 3-6. *Pump rate and electrical conductivity of the pumped water from KXTT4:S4 during test CX-2.*

Test CX-2 included measurements of flow rates using the tracer dilution method in twelve selected observation sections. The measurements were performed both under natural gradient and during pumping of section KXTT4:S4 (Feature B) in order to study the influence of the pumping. The results presented in Table 3-3 show a distinct influence in most of the tested sections. Examples are shown in Figure 3-7.

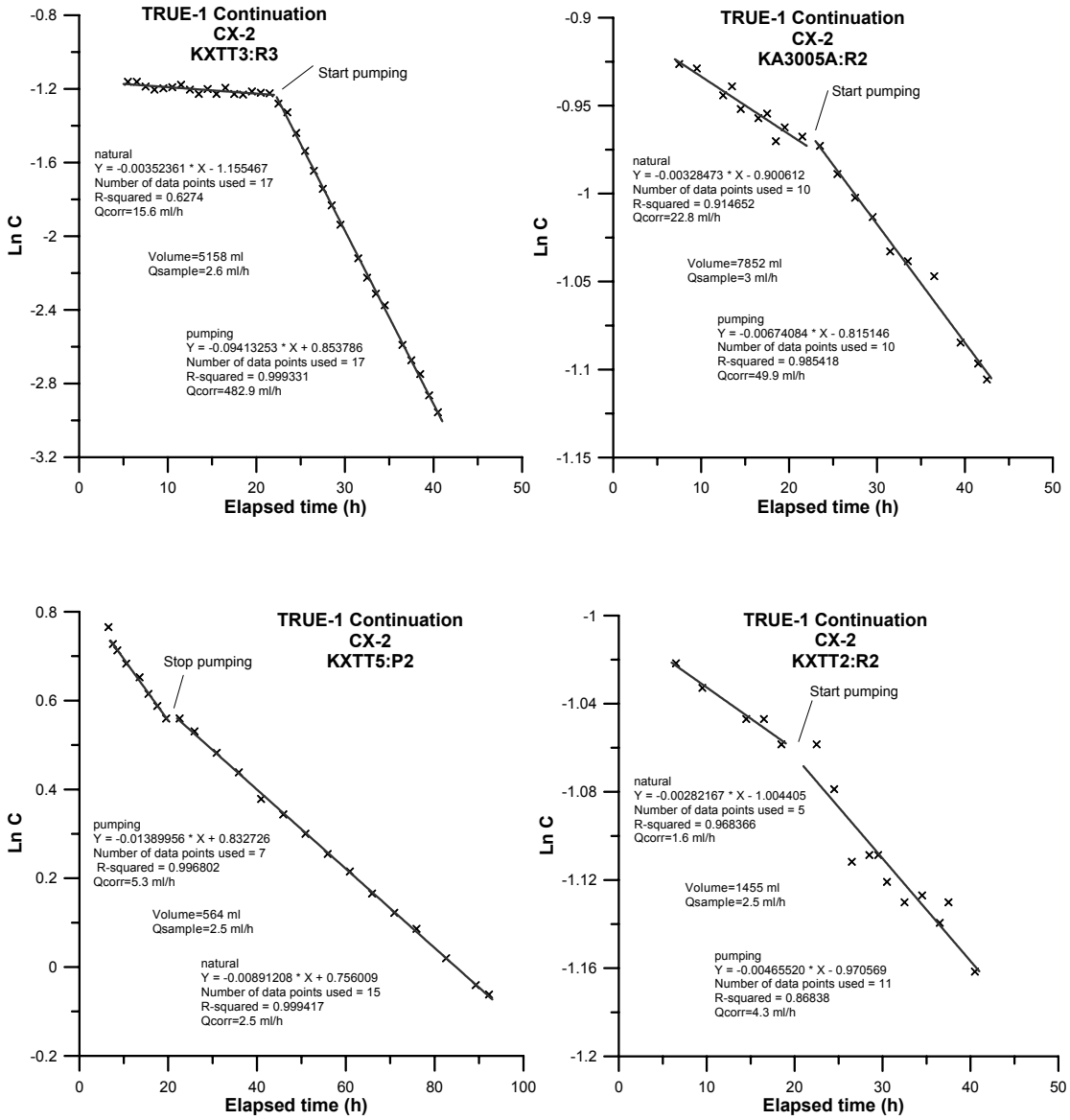

Figure 3-7. *Examples of tracer dilution graphs (Logarithm of concentration versus time) for sections KXTT3:R3 (Feature B), KA3005A:P2 (Feature B), KXTT5:P2 (Feature A) and KXTT2:R2 (Feature A), test CX-2. Steeper dip of the straight-line fit implies a higher flow rate.*

Table 3-3. Results of tracer dilution tests during test CX-2 using KXTT4:S4 (Feature B) as sink.

Test section	Feature	Section volume (ml)	$Q_{natural}$ (ml/h)	Q_{pump} (ml/h)	ΔQ (ml/h)
KXTT1:R2	A	1466	2	6	+4
KXTT1:R3	B	8181	122	2050	+1928
KXTT2:R2	A	1455	2	4	+2
KXTT2:R3	B	4205	31	104?	+73
KXTT3:R2	A	1821	148	376	+228
KXTT3:R3	B	5158	16	483	+467
KXTT4:S2	A’	1414	3	4	+1
KXTT4:S3	A	1156	3	2	-1
KXTT4:S4	B	4985		SINK	
KXTT5:P2	A	564	2	5	+3
KA3005A:R2	B	7852	23	50	+27
KA3005A:R3	A	2192	0.2	2	+1.8
KA3010A:P2	NW-2	13742	831	211?	-620

3.5 Test CX-3

Test CX-3, performed by pumping borehole section KXTT3:R2 (Feature A), shows pressure responses (>1 kPa) in totally 41 borehole sections within and outside the TRUE-1 array over distances ranging between 3 and 166 m. The radius of influence of this test is significantly larger than tests CX-1 and CX-2 due to the higher pumping rate (about 5 times higher).

The responses presented in Figure 3-8 are clearly separated in three classes. The first, showing high, and in most cases fast, responses, belong to sections associated with Feature A and, as in CX-1, also sections KA3005A:R4 and R5. The second class includes all the remaining sections in the TRUE-1 array while the third class shown in Figure 3-8 are the far distant boreholes, where KA3067A seem to respond best, possibly due to the previously interpreted bounding fracture zones NW-3 and NW-2. Responses could also be noted as far as about 150 m away in boreholes HA1960A, KA3105A and KA3110A possibly through fracture zone NNW-4, c.f. Figure 2-2.

The flow rate was rather constant between 2.60 and 2.64 l/min during the pumping period of CX-3, cf. Figure 3-9. A decrease in electrical conductivity indicating increasing portion of less saline water was also noted.

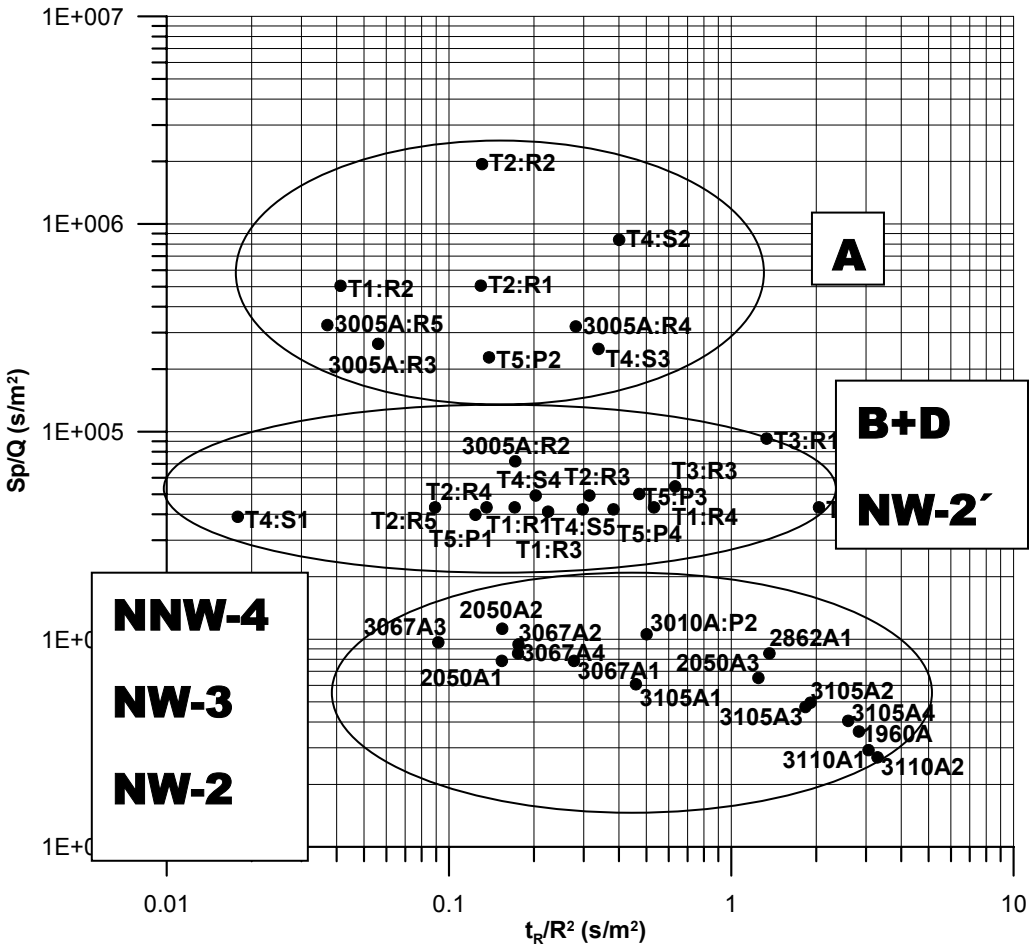

Figure 3-8. *Diagnostic plot of pressure responses during test CX-3. The encircled areas mark the responses of different Features. Borehole notations are shortened by removing the prefix "KXT-" and "KA-" from the borehole labels, cf. Table 2-1.*

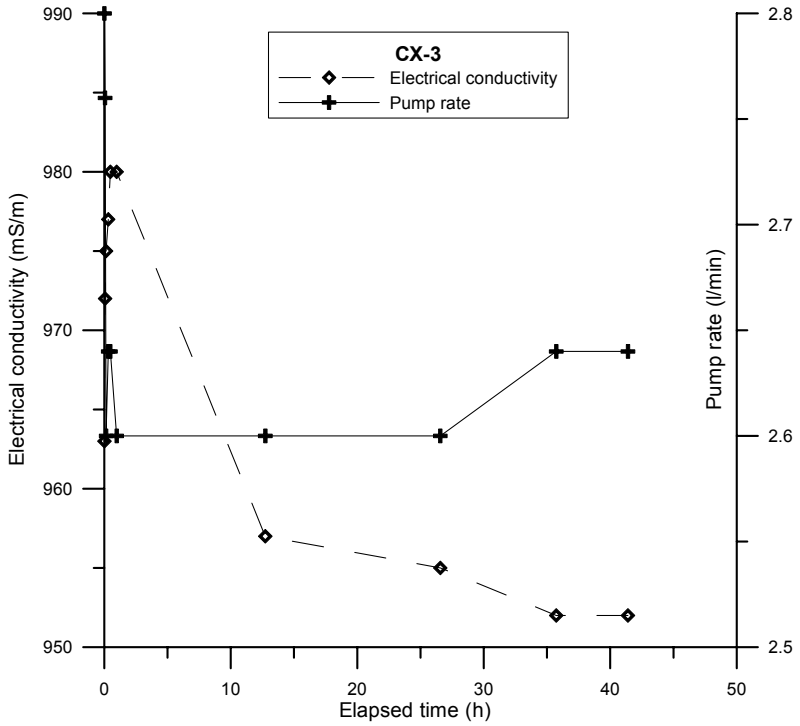

Figure 3-9. *Pump rate and electrical conductivity of the pumped water from KXTT3.R2 during test CX-3.*

Test CX-3 included measurements of flow rates using the tracer dilution method in twelve selected observation sections. The measurements were performed both under natural gradient and during pumping of section KXTT3:R2 (Feature A) in order to study the influence of the pumping. The results presented in Table 3-4 show a distinct influence in all of the tested sections. Examples are shown in Figure 3-10.

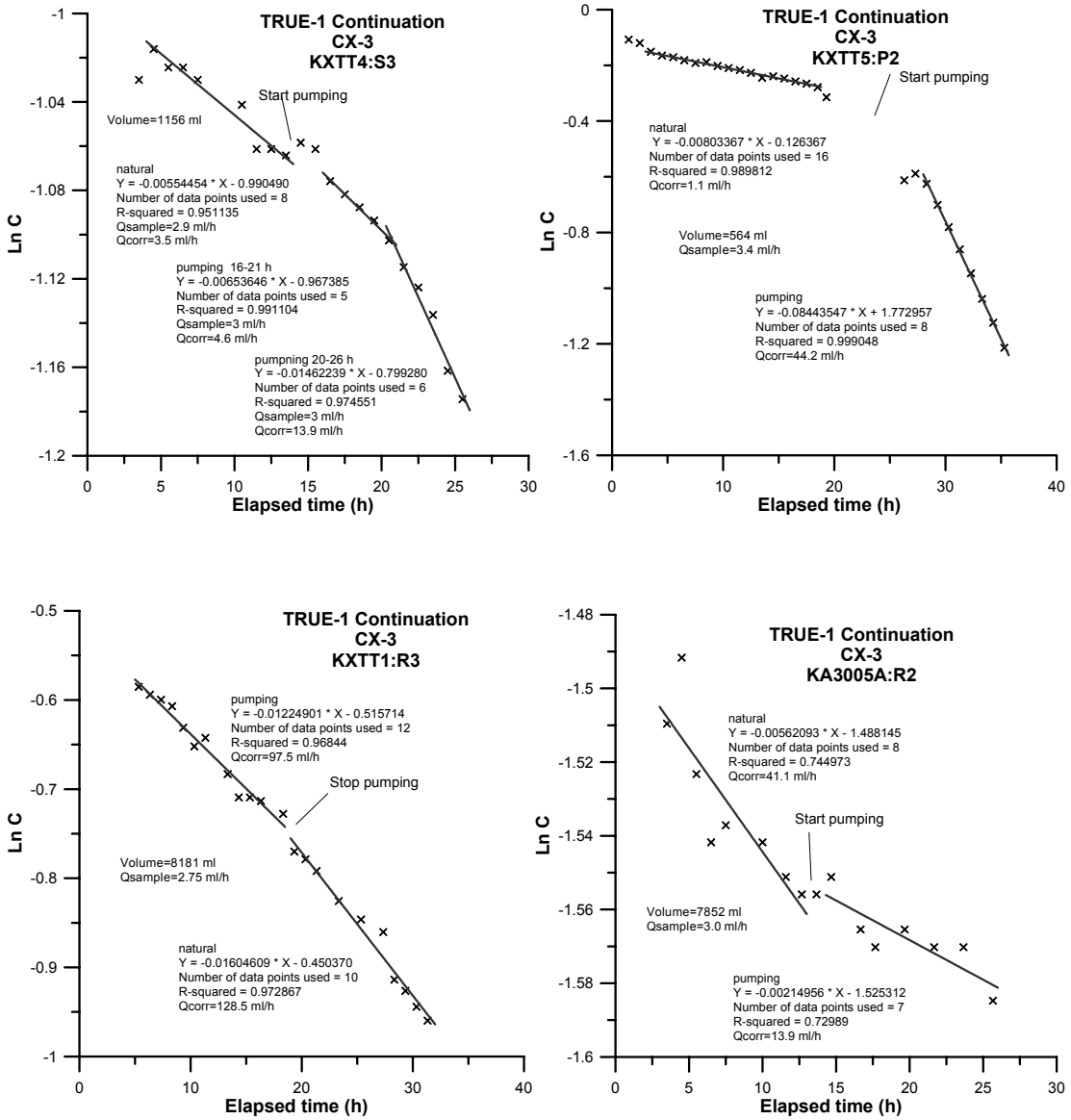

Figure 3-10.*Examples of tracer dilution graphs (Logarithm of concentration versus time) for sections KXTT4:S3 (Feature A), KKTT5:P2 (Feature A), KXTT1:R2 (Feature B) and KA3005A:R2 (Feature B), test CX-3. Steeper dip of the straight-line fit implies a higher flow rate.*

Table 3-4. Results of tracer dilution tests during test CX-3 using KXTT3:R2 (Feature A) as sink.

Test section	Feature	Section volume (ml)	$Q_{natural}$ (ml/h)	Q_{pump} (ml/h)	ΔQ (ml/h)
KXTT1:R2	A	1466	2?	574	+572
KXTT1:R3	B	8181	129	97	-32
KXTT2:R2	A	1455	7	25	+18
KXTT2:R3	B	4205	36	14	-22
KXTT3:R2	A	1821		SINK	
KXTT3:R3	B	5158	17	28	+11
KXTT4:S2	A’	1414	2	0.2	-1.8
KXTT4:S3	A	1156	4	14	+10
KXTT4:S4	B	4985	292	196	-96
KXTT5:P2	A	564	1	44	+43
KA3005A:R2	B	7852	41	14	-27
KA3005A:R3	A	2192	0.8	1.3	+0.5
KA3010A:P2	NW-2	13742	882	1084	+202

3.6 Test CX-4

Test CX-4 was performed as a cross-hole tracer test using KXTT3:R2 as sink. Injections were made in KXTT4:S2 and KXTT4:S3. The test was performed in a radially converging flow field with a constant withdrawal rate of Q=0.2 l/min in KXTT3:R2.

3.6.1 Tracer injections

At first, injections were made in borehole sections KXTT4:S2 (Uranine) and KXTT4:S4 (Amino G Acid) with concentrations in injection section of 100 mg/l and 400 mg/l respectively (CX-4a). When no breakthrough could be clearly detected in the sink section it was decided to repeat the injections but using higher tracer concentrations in the injection sections (CX-4b). At this time concentrations of about 1000 mg/l for both Uranine in KXTT4:S2 and Rhodamine WT in KXTT4:S3 were used.

The injections were performed as decaying pulses. The injection concentrations and injection rates given in Table 3-5 are the actually measured ones.

Table 3-5. Tracer injection data for test CX-4 (measured values).

Test	Inj. Section	Feature	Tracer	Max inj. conc. (mg/l)	Inj. rate (ml/h)	Inj. mass* (mg)	Section volume (ml)
CX-4a	KXTT4:S2	A’	Uranine	90	0.2	170	1414
CX-4a	KXTT4:S3	A	Amino-G Acid	399	1.3	490	1156
Cx-4b	KXTT4:S2	A’	Uranine	981	0.2	384	1414
CX-4b	KXTT4:S3	A	Rhodamine WT	792	0.6	1080	1156

*calculated by weighing

3.6.2 Tracer breakthrough

The flow in the injection sections turned out to be substantially lower than expected based on results from earlier performed tests (RC-1, STT-2). This resulted in difficulties to detect the tracer in the withdrawal section from the first injection (CX-4a) due to the about 20-100 times lower injection flow rates. One of the tracers, Uranine injected in KXTT4:S2, could be detected, but the other, Amino G Acid injected in KXTT4:S3 could only be indicated qualitatively from spectrofluorescence measurements.

When the injection was repeated with higher injection concentrations (CX-4b), breakthrough from both tracers was observed, Figures 3-11 and 3-12. The first peak of the breakthrough curve (Uranine) from KXTT4:S2 is resulting from remnants of the previous tracer injection (CX-4a) in the same section.

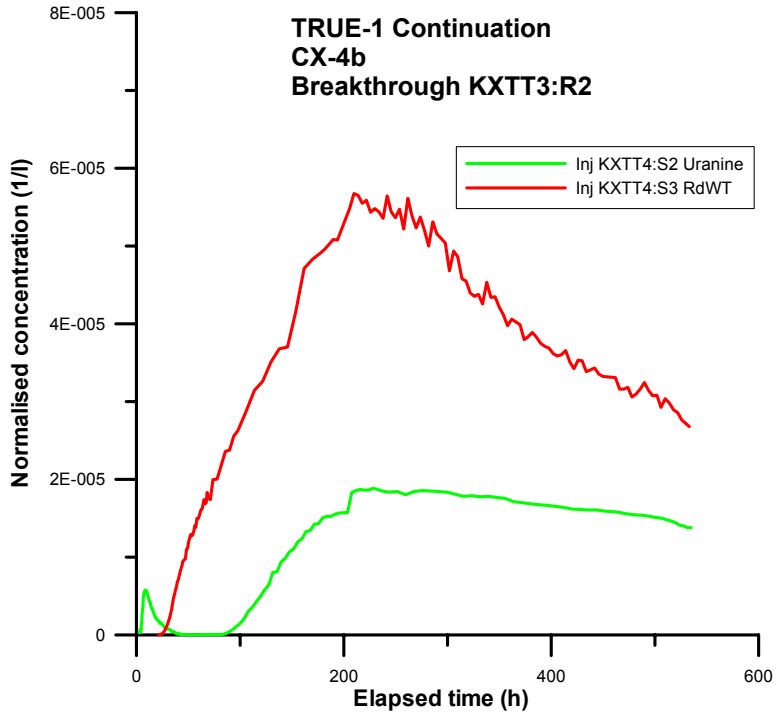

Figure 3-11. *Tracer breakthrough curves test CX-4b, injection in KXTT4:S2 (green) and KXTT4:S3 (red), linear scale.*

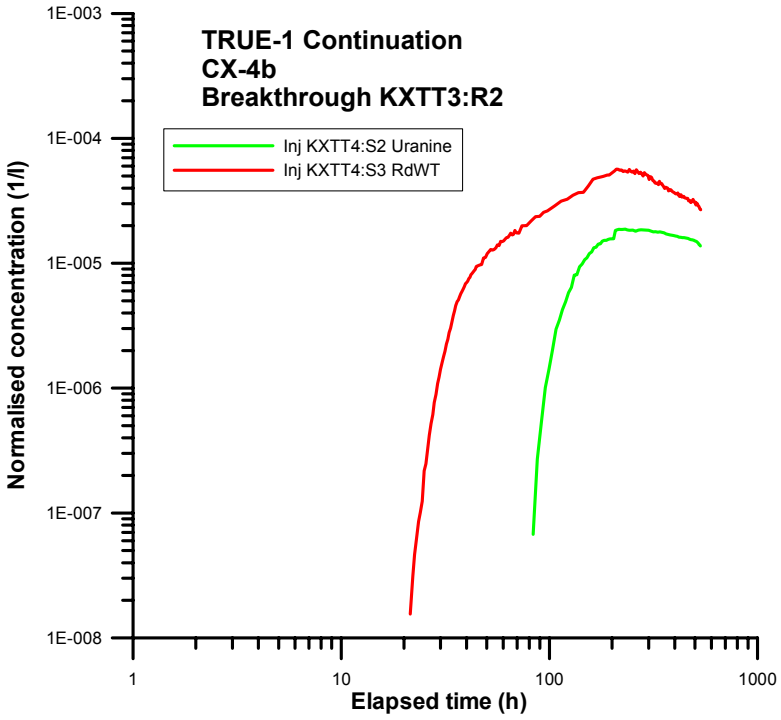

Figure 3-12. *Tracer breakthrough curves test CX-4b, injection in KXTT4:S2 (green) and KXTT4:S3 (red), logarithmic scale (first peak from inj in KXTT4:S2 excluded).*

Tracer mass recovery, presented in Table 3-6, was calculated by integrating the breakthrough curves for mass flux (mg/h) versus time (h) in the pumping borehole section. The injected mass was calculated by weighing the tracer solution vessel during the injection procedure. The low mass recovery (around 30%) is mainly due to the fact that sampling was stopped at a time when a large part of the mass still was moving along the flow path. An extrapolation of the breakthrough curves indicates that most of the mass would be recovered if pumping and sampling would have continued.

Table 3-6. Tracer mass recovery in pumping section KXTT3:R2 during test CX-4b.

Inj. section	Feature	Tracer	Recovery (%)	Sampling time (h)
KXTT4:S2	A’	Uranine	31	535
KXTT4:S3	A	Rhodamine WT	27	533

3.6.3 Numerical modelling and analytical interpretation

The breakthrough curves from CX-4b were evaluated using the one-dimensional advection-dispersion model described in Chapter 2.4.3.

The best-fit runs for each tracer/flow path are shown in Figure 3-13 and the parameters determined from the model runs are presented in Table 3-7. The regression statistics show low standard errors (1 %) except for the dispersivity with an error of 6-11 %. The transport parameters derived from the numerical modelling and the analytical expressions described in Chapter 2.4.3 are presented in Table 3-11 together with the results from test CX-5. The mean travel for the two flow paths (Features A and A´) are similar, indicating that the double-peak obtained during STT-2 may be explained by transport through two separate flow paths featured by small differences in transport properties. It should however be noted that the dispersivities for the two paths are significantly different.

Table 3-7. Evaluated parameters for CX-4b using PAREST (one-dimensional advection-dispersion model), cf. Chapter 2.4.3. Values within brackets are standard errors in percent.

Inj.section/Tracer	v (m/s)	t_m (h)	D/v (m)	F
KXTT4:S2, Uranine	$9.26 \cdot 10^{-6}$ (1)	140.3	0.14 (11)	$2.94 \cdot 10^{-5}$ (1)
KXTT4:S3, RdWT	$1.33 \cdot 10^{-5}$ (1)	97.5	1.16 (6)	$1.21 \cdot 10^{-4}$ (1)

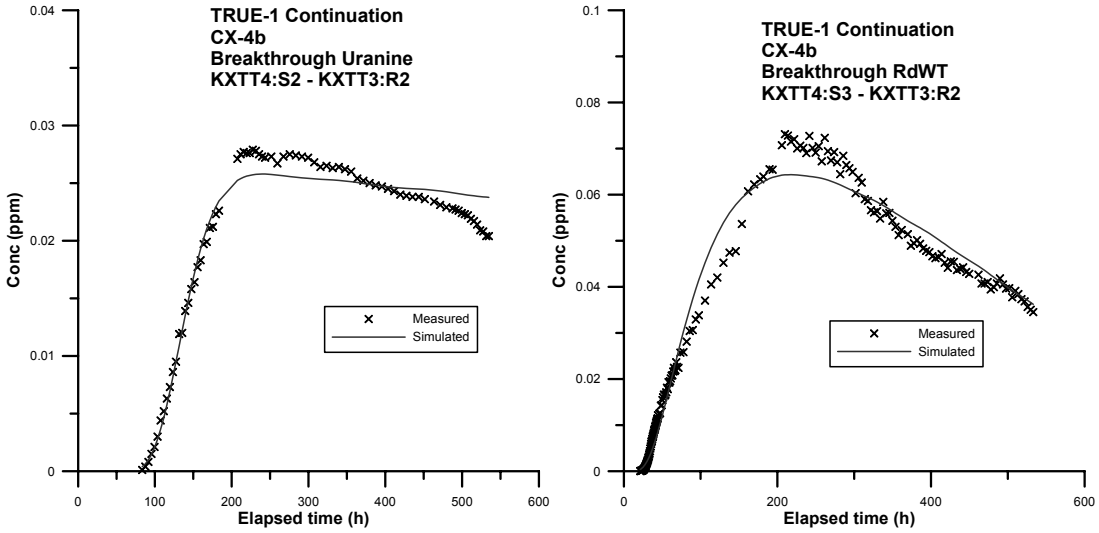

Figure 3-13. *Model simulations of breakthrough curves in test CX-4b.*

3.7 Test CX-5

Test CX-5 was performed as a cross-hole tracer test using KXTT3:R2 (Feature A) as sink. Injections were made in four sections, KXTT1:R2 and KXTT4:S3 in Feature A and KXTT1:R3 and KXTT4:S4 in Feature B, cf. Figure 3-14. The test was performed in a radially converging flow field with a constant withdrawal rate of Q=2.97 l/min in KXTT3:R2. The reason for using this high flow was to enable tracer breakthrough from Feature B, which is located in the opposite direction of the natural gradient, which is directed towards the tunnel.

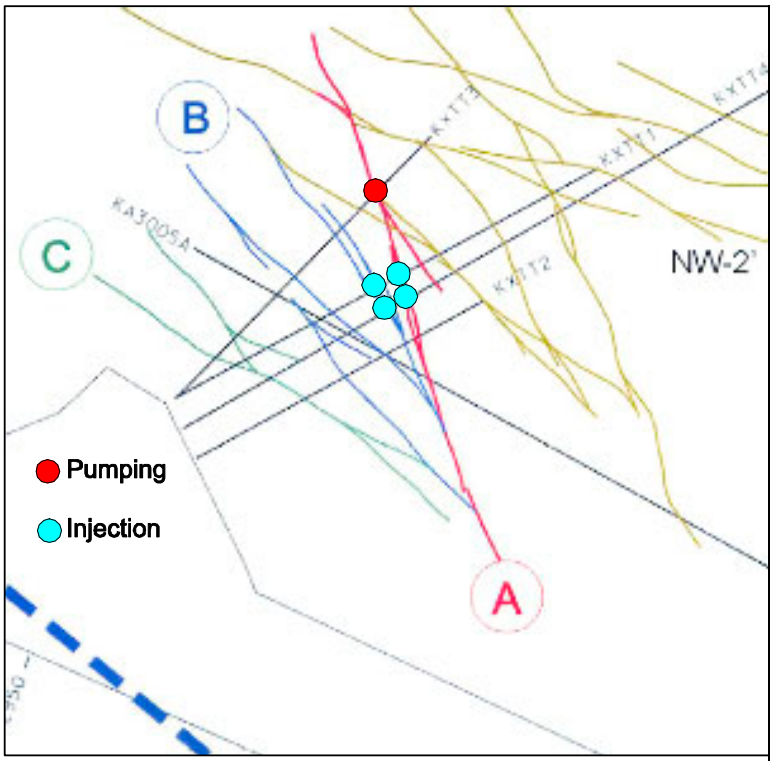

Figure 3-14. *Horizontal section at Z=–400 masl showing structural model based on identified conductive geological structures in the TRUE-1 rock volume and location of pumping and injection sections in test CX-5.*

The injections in KXTT1:R2 and KXTT4:R3 invokes the same experimental geometry as in the previously performed tracer tests STT-1, STT-1b and STT-2 (c.f. Winberg et al., 2000).

3.7.1 Tracer injections

The injections were performed as decaying pulses. The injection concentrations and injection rates given in Table 3-8 are the actually measured ones. The evaluated tracer injection flow rates are significantly higher than in test CX-4 (Table 3-5) due to the 15 times higher pumping rate in KXTT3:R2.

Table 3-8. Tracer injection data for test CX-5 (measured values).

Inj. Section	Feature	Tracer	Max inj. conc. (mg/l)	Inj. rate (ml/h)	Inj. mass* (mg)	Section volume (ml)
KXTT1:R2	A	Uranine	111	727	320	1466
KXTT1:R3	B	Uranine	1058	85	7702	8181
KXTT4:S3	A	Amino-G Acid	856	21	1226	1156
KXTT4:S4	B	Rhodamine WT	1055	185	5348	4985

*calculated by weighing

3.7.2 Tracer breakthrough

Tracer breakthrough was only detected from the two injections in Feature A, while no breakthrough could be detected from the two injections in Feature B after about 28 days of sampling (650 hours). The breakthrough curves (Figures 3-15 and 3-16) show a very fast transport as expected due to the high withdrawal rate in the pumping section. The lack of breakthrough from the injections in Feature B, although the distances from the injection points are similar for all 4 injections (about 5 m), indicates that no fast interconnecting flow paths exists between the two Features within the borehole array. However, it is still clear from the pressure interference test responses that the features are connected. Most likely in a manner as indicated by the current hydro-structural model (Figure 3-14). This implies travel distances in the order of about 20 m instead of the shortest (Euclidean) distance of about 5 m.

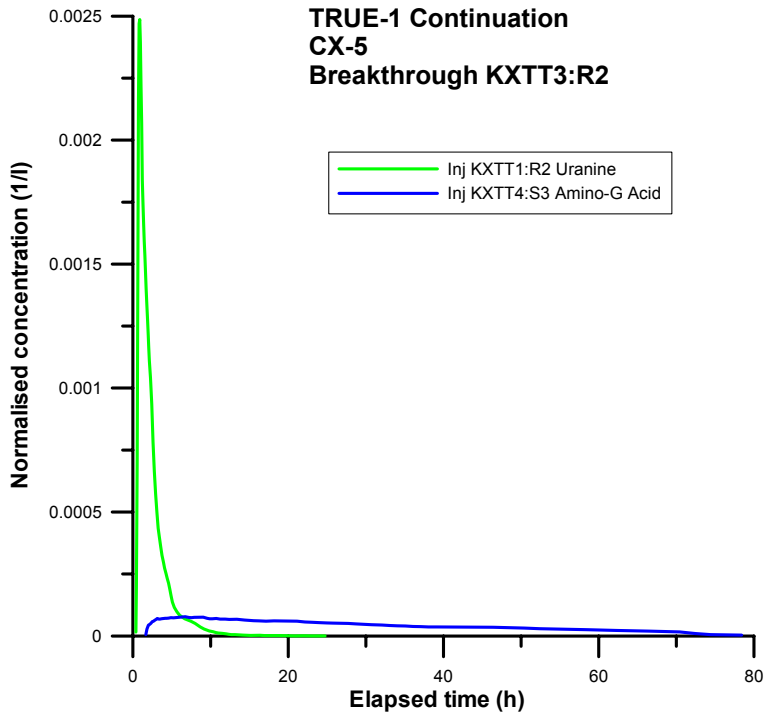

Figure 3-15. *Tracer breakthrough curves test CX-5, injection in KXTT1:R2 (green) and KXTT4:S3 (blue), linear scale.*

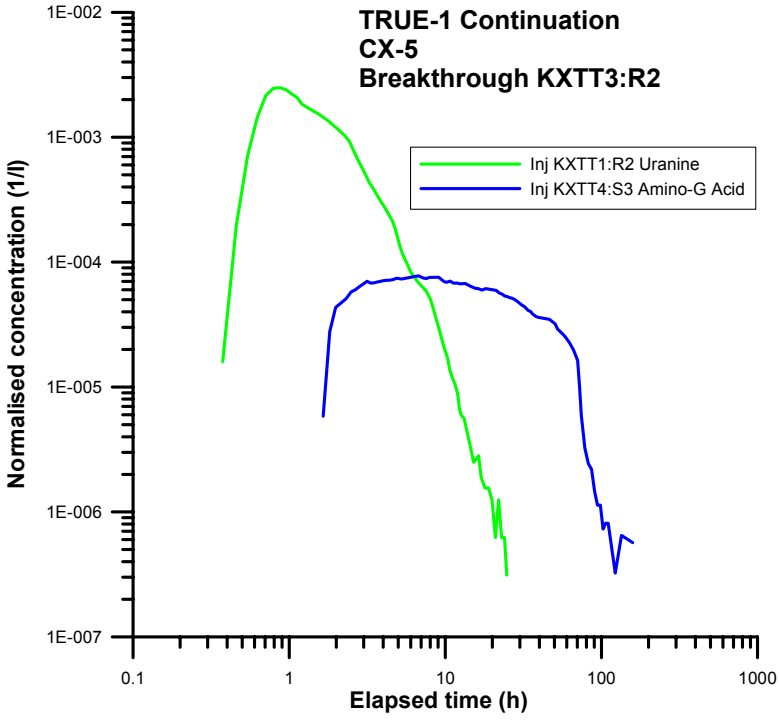

Figure 3-16. *Tracer breakthrough curves test CX-5, injection in KXTT1:R2 (green) and KXTT4:S3 (blue), logarithmic scale.*

Tracer mass recovery, presented in Table 3-9, was calculated by integrating the breakthrough curves for mass flux (mg/h) versus time (h) in the pumping borehole section. The injected mass was calculated by weighing the tracer solution vessel during the injection procedure.

Table 3-9. Tracer mass recovery in pumping section KXTT3:R2 during test CX-5.

Inj. Section	Feature	Tracer	Recovery (%)	Sampling time (h)
KXTT1:R2	A	Uranine	79	26
KXTT4:S3	A	Amino-G acid	56	158
KXTT1:R3	B	Uranine	no bt	640
KXTT4:S4	B	Rhodamine WT	no bt	663

no bt=no breakthrough

3.7.3 Numerical modelling and analytical interpretation

The breakthrough curves from CX-5 were evaluated using the one-dimensional advection-dispersion model described in Chapter 2.4.3.

The parameters determined from the model runs are presented in Table 3-10. The best-fit runs for each tracer/flow path are presented in Figure 3-17. It should be noted that the injection function is not fully characterized due the short travel time. This is possibly also an explanation for the relatively poor fit. The regression statistics show low standard errors (1-3 %) except for the dispersivity with an error of 21-23 %.

The transport parameters derived from the numerical modelling and the analytical expressions described in Chapter 2.4.3 are presented in Table 3-11 together with the results from test CX-4.

A summary of flow and transport parameters for all tests performed in the same flow paths as CX-5 is shown and discussed in Chapter 4.

Table 3-10. Evaluated parameters in CX-5 using PAREST (one-dimensional advection-dispersion model), cf. Chapter 2.4.3. Values within brackets are standard errors in percent.

Inj.section/Tracer	v (m/s)	t_m (h)	D/v (m)	F
KXTT1:R2, Uranine	$4.10 \cdot 10^{-3}$ (2)	0.34	0.17 (23)	$7.08 \cdot 10^{-3}$ (1)
KXTT4:S3, Amino-G	$8.01 \cdot 10^{-4}$ (3)	1.6	0.92 (21)	$1.24 \cdot 10^{-4}$ (1)

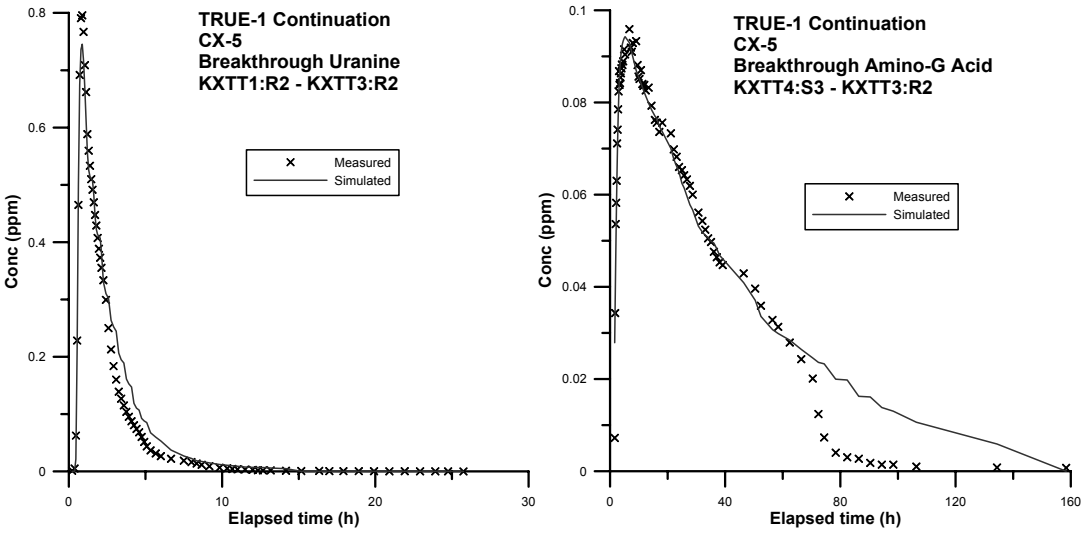

Figure 3-17. *Model simulations of breakthrough curves in test CX-5.*

Table 3-11. Summary of hydraulic and transport parameters for the flow paths tested in CX-4b and CX-5 using KXTT3:R2 as sink. Values within brackets are standard errors in percent.

Parameter	CX-4b KXTT4:S2	CX-4b KXTT4:S3	CX-5 KXTT1:R2	CX-5 KXTT4:S3	Source
Euclidian distance, L (m)	4.68	4.68	5.03	4.68	Geometry
Withdrawal rate, Q (l/min)	0.2	0.2	2.97	2.97	Measured
Mean head difference, Δh (m)	2.8	3.2	134.4	149.1	HMS
Inj. flow rate (ml/h)	0.2	0.6	727	21	Injection curve
Mean travel time, t_m (h)	140	97.5	0.34	1.6	PAREST
Mean velocity, v (m/s)	$9.26\cdot10^{-6}$ (1)	$1.33\cdot10^{-5}$ (1)	$4.10\cdot10^{-3}$ (2)	$8.01\cdot10^{-4}$ (3)	PAREST
First arrival, t_a (h)	90	23	0.3	1.6	BTC*
Peclet number, Pe	33	4.0	29	5.1	PAREST
Dispersivity, D/v (m)	0.14 (11)	1.16 (6)	0.17 (23)	0.92 (21)	PAREST
Fracture conductivity, K_{fr} (m/s)	$3.9\cdot10^{-5}$	$4.9\cdot10^{-5}$	$4.0\cdot10^{-4}$	$6.4\cdot10^{-5}$	Eq. 2-4
Equivalent fracture aperture, b (m)	$2.4\cdot10^{-2}$	$1.7\cdot10^{-2}$	$7.6\cdot10^{-4}$	$4.2\cdot10^{-3}$	Eq. 2-5
Flow porosity, θ_k (2 m thickness)	$3.5\cdot10^{-3}$	$2.8\cdot10^{-3}$	$2.6\cdot10^{-4}$	$1.6\cdot10^{-3}$	Eq. 2-6
Mass recovery, R (%)	31	27	79	56	BTC*

*BTC=Breakthrough curve

3.8 Supporting data

The head distribution in Feature A during the entire test period is shown in Figure 3-18. The influence of the pumping in different sections are clearly seen, see also Log of Events in Table 3-1.

A longer period with pumping in borehole section KXTT3:R2 starts on February 8th, Test CX-4. The withdrawal rate was stable and constant during the test, 0.2 l/min, and Figure 3-18 shows a slight decrease in head during the period. On March 18th the head drops about 5 meters in all sections and increases somewhat again on April 2nd. This is due to activities in borehole KA3065A03 at the neighbouring LTDE site.

Due to power failure the pumping stopped on April 6th. It was started again on April 9th and the pumping rate in KXTT3:R2 was increased to 2.97 l/min for test CX-5. A packer failure occurs in borehole KXTT5 on April 23rd due to a leakage in the inflation system. Examination of the pressure registrations from KXTT5 shows that the hydraulic head increases in all sections due to short-circuiting, as the pressure is governed by the inner high transmissive parts of the borehole (Feature NW-2). The effect on Features A and B are small or even negligible in the pumping section. In general, the hydraulic head increases about 8 metres both in Feature A and B but the direction and magnitude of the hydraulic gradient is not changed to any significant degree. On May 6th the packers in KXTT5 are re-inflated and the hydraulic head situation restored. The pumping is stopped on May 14th and the test period is ended.

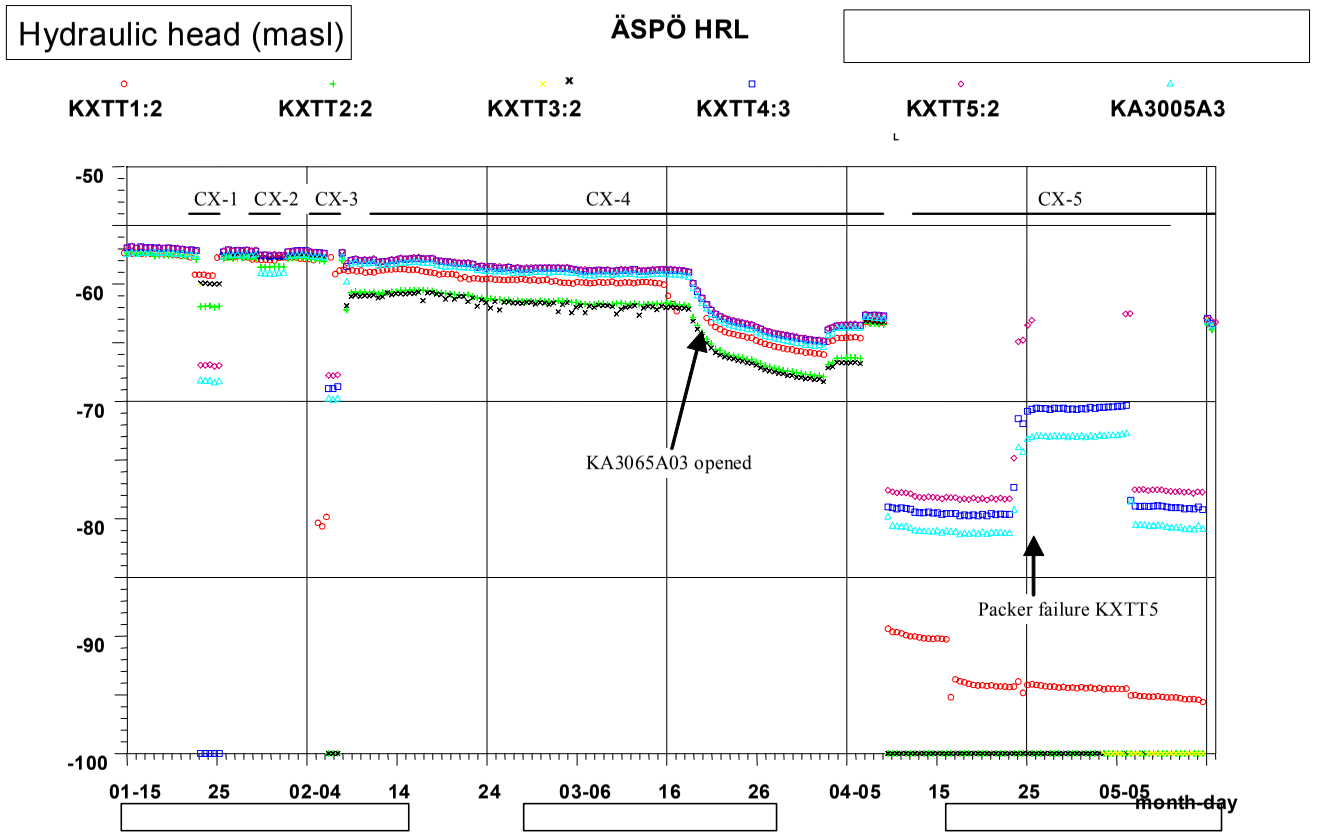

Figure 3-18. *Hydraulic head in Feature A during TRUE-1 Continuation tests CX-1 - CX-5, January 15th to May 15th, 2002.*

4 Discussion and conclusions

4.1 Connectivity and structural model

In general, the performed tests confirm the existing hydro-structural model (Winberg et al., 2000.

The pressure interference tests CX-1 and CX-3, using Feature A as sink, show similar response patterns, with high and fast responses in sections interpreted to include Feature A and fast but significantly lower responses in sections including the bounding fracture zone NW-2. Features B and D responds lower and slower.

The large drawdown created during test CX-3 induces responses also in the bounding fracture zones NNW-4, NW-2 and NW-3, in particular in borehole KA3067A (Zones NW-2 and NW-3). There are only a few responses that do no follow the pattern described above, in particular the very good responses in sections KA30005A:R4, KA30005A:R5 and KXTT2:R1. These responses indicate that splay fractures to Feature A are present.

The re-instrumentation and subsequent testing of borehole KXTT4, where the section enclosing Feature A (section R3) was divided into two sections (S2 and S3) by means of a packer, clearly shows that section S2 includes a possible splay fracture to Feature A.

The determination of flow rates using the tracer dilution method performed both under natural (ambient) gradient and during the pumping phase of tests CX-1 to CX-3 also confirms the hydro-structural model presented by Winberg et al. (2000). Each test included flow measurements of 12 sections and significant flow responses were noted in all three tests and in almost all sections measured. The magnitude of flow and flow responses are governed by the local transmissivity of the borehole section and the hydraulic gradient. Thus, flow rates vary by three orders of magnitude (c.f. Tables 3-2 to 3-4).

Test CX-1 show significant responses in all but two sections (Table 3-2). Only three sections show increased flow while the rest show decreased flow rate. This is consistent with the prevailing hydraulic gradient where sections located at a “down gradient” position in relation to the pumping section gets a reversal or partly reversal of the flow direction whereas section placed “up gradient” always shows an increase of flow. A similar pattern was noted during test CX-3 (Table 3-4) but due to the large drawdown, many of the sections show increased flow rates (7 out of 12).

Test CX-2 in Feature B generally show increased flow rates as the pumped section (KXTT4:S4) is located “down gradient” compared to Feature A.

The general conclusion that can be drawn from the results of the pressure interference tests and tracer dilution tests is that the TRUE-1 array consists of at least three well separated hydraulic units, Feature A, Feature B+D and Feature NW-2. This conclusion is also supported by tracer test CX-5 where no tracer transport between Features A and B could be detected. Hence, the flow regime may not be considered as three-dimensional in the scale of the tracer tests (up to 10 metres). In a larger scale it is obvious that the features are interconnected.

4.2 Boundary conditions

The large-scale boundary conditions at the TRUE-1 site have slowly and gradually changed over the years since the project started in 1995. Källgården et al. (2002) have studied the evolution of water inflow, pressure and water chemistry at the site as a pre-study to TRUE-1 Continuation. They conclude that inflow to the tunnel section at the site and the groundwater pressures has decreased significantly during the period 1995 to June 2001 and that the pressures decrease faster closer to the tunnel, possibly due to emptying of the water storage close to the tunnel. This implies that the difference in hydraulic head between Features A and B also increases over time and the situation during tracer tests CX-4 and CX-5 was that the natural head difference between the features was around 15 m compared to about 10 m during the performance of tests STT-1 and STT-2 in 1997, cf. Table 4-1.

The head distribution within Feature A however, is virtually unchanged. Table 4-1 and Figure 4-1 shows the prevailing natural hydraulic head in Feature A compared to the one before starting the sorbing tracer tests in June 1997. The hydraulic head has decreased about 4 meters since then but the head difference between the highest and lowest has decreased from about 1 m to about 0.6 m implying a somewhat lower hydraulic gradient (about 6%). A comparison of the two head maps in Figure 4-1 shows that the direction of the hydraulic gradient has changed somewhat to be more downward.

Feature B shows larger head differences and a similar direction of the natural gradient. The intercept in borehole KA3005A is clearly influenced by the closeness and possible intersection with Feature A (see Figure 2-2) which also is manifested during pumping in Test CX-3 where the head difference between Features A and B decreases to only about 1.7 m.

Table 4-1. Hydraulic head (masl) in sections containing Feature A during natural conditions and during pumping in KXTT3:R2 during test CX-3 to CX-5.

Borehole Section	Natural head June 1997	Natural head Jan 2002	Induced head test CX-4*	Induced head test CX-3 and CX-5
Feature A				
KXTT1:R2	-53.0	-57.4	-58.9	-80.0
KXTT2:R2	-53.0	-57.4	-60.6	-146.4
KXTT3:R2	-52.6	-57.1	-60.9	-173.3
KXTT4:R3	-52.9	-56.9 (S3)	-58.1 (S3)	-68.8 (S3)
KXTT5:P2	-	-56.8	-57.9	-67.7
KA3005A:R3	-53.6	-57.5	-58.4	-69.8
Feature B				
KXTT1:R3	-64.6	-75.1	-75.6	-77.1
KXTT2:R3	-62.6	-74.5	-75.4	-77.1
KXTT3:R3	-61.1	-70.8	-72.8	-75.1
KXTT4:R4	-61.4	-72.2	-73.4	-75.3
KXTT5:P3	-	-66.6	-67.6	-69.6
KA3005A:R2	-59.9	-67.7	-68.4	-71.5

* prior to opening of KA3065A03

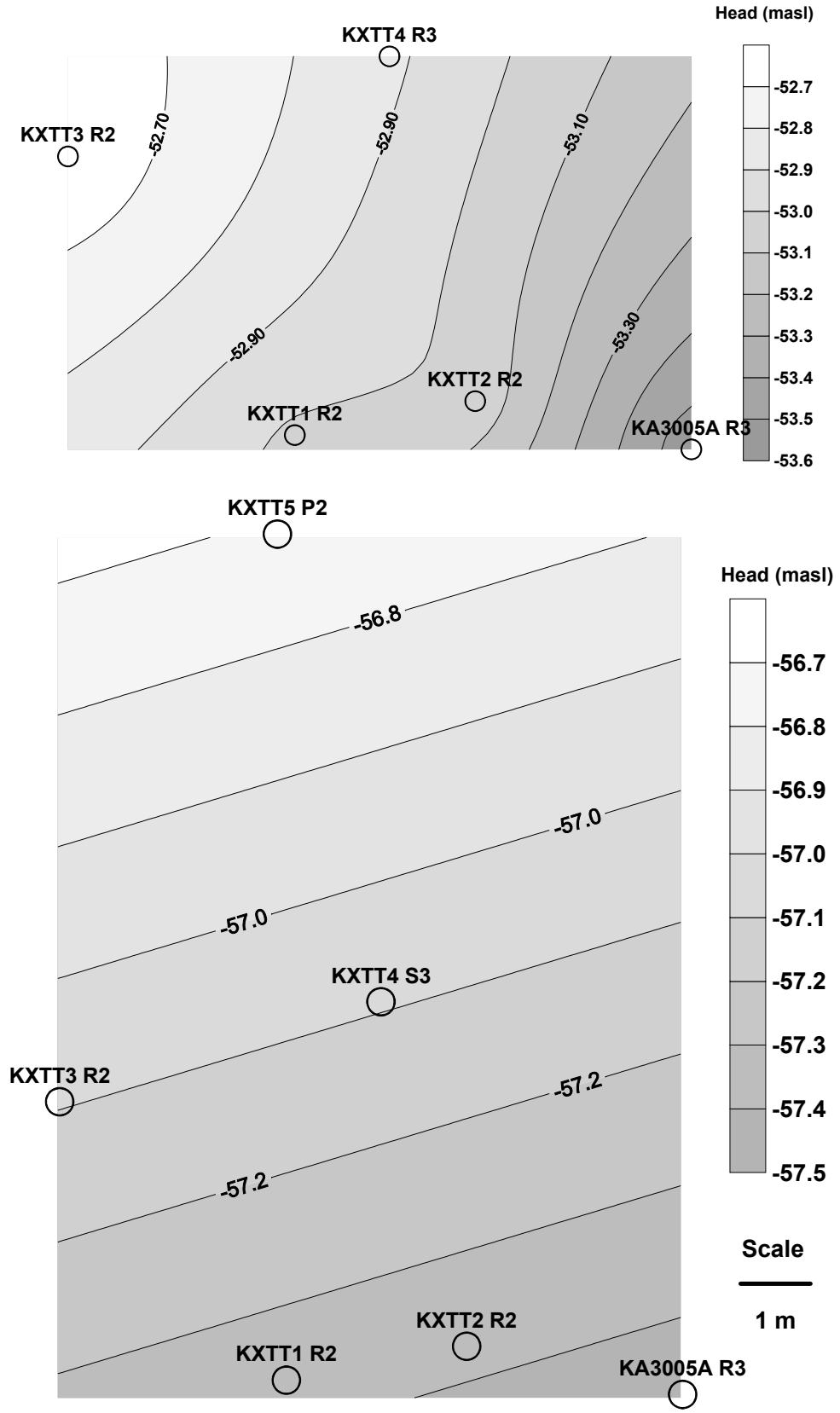

Figure 4-1. *Hydraulic head distribution in Feature A before the sorbing tracer tests in June 1997 (upper graph) and before the TRUE-1 Continuation tests in January 2002 (lower graph). Interpolated point data (SURFER™). Borehole KXTT5 had not been drilled in June 1997.*

4.3 Transport and evaluated parameters

The tracer test CX-4b was performed with the aim to explore the cause of the double peak observed in the breakthrough curves obtained during the test STT-2 (Andersson et al., 1999a). Test CX-4b, performed by pumping in borehole section KXTT3:R2 (Feature A) with a rate of 0.2 l/min (same as in STT-2) resulted in breakthrough from both injection points, KXTT4:S2 and KXTT4:S3, both in Feature A.

The breakthrough curves from test CX-4b show:

- Feature A is divided in two separated fractures at the intersection with KXTT4 (sections S2 and S3) where Feature A´ (section S2) may be a possible splay fracture to Feature A.

- The travel times are similar, which explains why they could not be separated as two distinct flow paths in test RC-1 and STT-1. Subtle changes in the boundary conditions during test STT-2 caused a slight difference in travel time for the two flow paths as suggested by Winberg et al. (2000).

- The evaluated tracer mass recovery is 31% for Uranine (KXTT4:S2) and 27% for Rhodamine WT (KXTT4:S3) after 530 hours of sampling.

- Results from modelling using a one-dimensional advection-dispersion model show significantly lower dispersivities (D/v = 0.14 and 0.16) for both flow paths than for the "combined" flow path evaluated in STT-1 and RC-1 (D/v = 2 m), cf. Table 4-3.

- Mean travel times for the two flow paths (97 and 140 hours) are significantly longer than during STT-2 (8 and 26 hours) although the same strength of the sink was applied.

- The slower transport is possibly an effect of changed boundary conditions and/or altered hydraulic characteristics for the flow path. The calculated hydraulic conductivity of the fracture is about one order of magnitude lower than in the previously performed tests (Table 4-1). This is also shown by the low injection flow rates (Table 3-5) which are about 20-100 times lower than in STT-2. This may be a possible indirect indication of mobilisation of uncohesive material.

The tracer test CX-5 was performed with the purpose to assess connectivity between Feature B and A. Test CX-5 was performed in a radially converging flow field with a constant withdrawal rate of Q=2.97 l/min in KXTT3:R2. Injections were made in four sections, KXTT1:R2 and KXTT4:S3 in Feature A and KXTT1:R3 and KXTT4:S4 in Feature B. Tracer breakthrough was only detected from the two injections in Feature A, while no breakthrough could be detected from the two injections in Feature B.

Evaluation of the results from CX-5 shows:

- The mean travel times are very short, 0.3 and 1.6 hours, respectively.
- Tracer mass recovery of about 80% for Uranine (KXTT1:R2) and 56% for Amino G (KXTT4:S3) after 150 hours of sampling. The value for Amino G is somewhat low but also uncertain due to high background.
- Results from modelling using a one-dimensional advection-dispersion model show a similar value of dispersivity for KXTT4:S3 as in CX-4b and a somewhat lower dispersivity for the flow path KXTT1:R2 – KXTT3:R2 than previously evaluated (STT-1b), 0.2 m compared to 0.5 m, cf. Table 4-4. However, it should also be noted that the injection function is not fully characterized due the short travel time. It is also likely that the flow path is much narrower and less dispersed due to the extremely large gradient employed. This is also indicated by the lower values of equivalent fracture aperture and flow porosity than evaluated from previous runs (cf. Table 4-4).
- A packer failure occurred in KXTT5 after about 200 hours of injection. This has no effect on the breakthrough from Feature A, but may potentially have had an effect on transport from Feature B. Examination of the pressure registrations from KXTT5 shows that the hydraulic head increases in all sections due to short-circuiting, as the high transmissive parts are in the inner parts of the borehole. The effect on Features A and B are small, or even negligible, in the pumping section. In general, the hydraulic head increases about 8 metres both in Feature A and B but the direction and magnitude of the hydraulic gradient is not changed to any significant degree.
- The lack of breakthrough from Feature B after 700 hours of pumping indicates that no short-circuiting 3D-network of conducting fracture exists in the TRUE-1 target area. There is still a possibility that a connection between the features exists as indicated by the structural model but it is likely that such a flow path is much longer than the Euclidean distance between the pumping in Feature A and the injection points in Feature B which is 4.8 and 5.4 metres, respectively. This is also consistent with the separated pressure response pattern revealed during pressure interference tests CX-1 through CX-3.

Table 4-3. Summary of flow and transport parameters determined for the flow path KXTT4:R3 → KXTT3:R2 (distance 4.68 m).

Test	Q (l/min)	Δh (m)	R (%)	D/v (m)	K_{fr} (m/s)	b (m)	θ_k
RC-1	0.2 (0.4)$^{++}$	2.8 (6.9)$^{++}$	100	1.6	$7.1\cdot10^{-4}$	$1.4\cdot10^{-3}$	$0.5\cdot10^{-3}$
DP-5	0.1	3.0	28	0.34	$2.0\cdot10^{-4}$	$1.6\cdot10^{-3}$	$0.5\cdot10^{-3}$
DP-6	0.2	3.6	70	0.48	$4.1\cdot10^{-4}$	$2.4\cdot10^{-3}$	$0.4\cdot10^{-3}$
PDT-1	0.1	1.0	74	0.6	$6.4\cdot10^{-4}$	$2.1\cdot10^{-3}$	$0.5\cdot10^{-3}$
PDT-2	0.2	2.3	99	1.1	$5.9\cdot10^{-4}$	$2.0\cdot10^{-3}$	$0.6\cdot10^{-3}$
PDT-3	0.4	6.8	95	1.7	$4.8\cdot10^{-4}$	$1.7\cdot10^{-3}$	$0.7\cdot10^{-3}$
STT-1	0.4	7.2–10.5	100	2.0	$4.2\cdot10^{-4}$	$1.4\cdot10^{-3}$	$0.8\cdot10^{-3}$
STT-2	0.2	5.6–8	88	0.35*	$3.4\cdot10^{-4*}$	$1.3\cdot10^{-3*}$	$1.1\cdot10^{-3*}$
STT-2				0.46**	$1.0\cdot10^{-4**}$	$4.5\cdot10^{-3**}$	$4.0\cdot10^{-3**}$
CX-4[1]	0.2	2.8	31	0.14	$3.9\cdot10^{-5}$	$2.4\cdot10^{-2}$	$3.5\cdot10^{-3}$
CX-4[2]	0.2	3.2	27	1.16	$4.9\cdot10^{-5}$	$1.7\cdot10^{-2}$	$2.8\cdot10^{-3}$
CX-5	2.97	149.1	56	0.92	$6.4\cdot10^{-5}$	$4.2\cdot10^{-3}$	$1.6\cdot10^{-3}$

$^{++}$ Pumping increased during experiment
* Flow path #1
** Flow path #2
[1] Injection section KXTT4:S2
[2] Injection section KXTT4:S3

Table 4-4. Summary of flow and transport parameters determined for the flow path KXTT1:R2 → KXTT3:R2 (distance 5.03 m).

Test	Q (l/min)	Δh (m)	R (%)	D/v (m)	K_{fr} (m/s)	b (m)	θ_k
PTT-1	0.87	24	95	(0.6)***	$3.5\cdot10^{-4}$	$1.4\cdot10^{-3}$	$1.0\cdot10^{-3}$
RC-1	0.2 (0.4)**	2.5 (5.6)**	93	0.24	$5.0\cdot10^{-4}$	$2.2\cdot10^{-3}$	$0.7\cdot10^{-3}$
DP-1	0.1	5.8	88	0.40	$2.8\cdot10^{-4}$	–	$1.2\cdot10^{-3}$
PDT-1	0.1	0.6	44	1.3	$11\cdot10^{-4}$	$2.1\cdot10^{-3}$	$0.4\cdot10^{-3}$
PDT-2	0.2	1.9	52	1.0	$5.6\cdot10^{-4}$	$2.6\cdot10^{-3}$	$0.7\cdot10^{-3}$
PDT-4	0.4	9.3	100	–	–	–	–
STT-1b	0.4	9.3–12.8	100	0.55	$1.8\cdot10^{-4}$	$1.8\cdot10^{-3}$	$1.1\cdot10^{-3}$
CX-5	2.97	134.4	79	0.17	$4.0\cdot10^{-4}$	$7.6\cdot10^{-4}$	$2.6\cdot10^{-4}$

** Pumping increased during experiment
*** Uncertain due to transport in equipment

References

Andersson, P., 1996: TRUE 1st stage tracer test programme. Experimental data and preliminary evaluation of the TRUE-1 radially converging tracer test (RC-1). Äspö Hard Rock Laboratory Progress Report HRL-96-24.

Andersson, P., Wass E., Byegård J., Johansson H., Skarnemark G., 1999a: TRUE 1st stage tracer test programme. Tracer tests with sorbing tracers STT-2. Experimental description and preliminary evaluation. Äspö Hard Rock Laboratory International Progress Report IPR-99-15.

Andersson, P., Ludvigson, J-E., Wass, E., Holmqvist, M., 1999b: TRUE Block Scale Project, Detailed Characterisation Stage. Interference tests and tracer tests, PT-1 - PT-4. Äspö Hard Rock Laboratory International Progress Report IPR-01-52.

Andersson P., Ludvigson J-E., Wass E., Holmqvist M., 2000: TRUE Block Scale Project Tracer Test Stage. Interference tests, dilution tests and tracer tests, Phase A. Äspö Hard Rock Laboratory International Progress Report IPR-00-28.

Andersson P., Byegård J., Winberg A., 2002: Final report of the TRUE Block Scale project. 2. Tracer tests in the block scale. SKB Technical Report TR-02-14.

Byegård, J., Johansson, H., Andersson, P., Hansson, K., Winberg, A., 1999: Test plan for the long term diffusion experiment. Äspö Hard Rock Laboratory International Progress Report IPR-99-36.

Cooper, H.H. Jr., Jacob, C.E., 1946: A Generalized Graphical Method for Evaluating Formation Constants and Summarizing Well-Field History. Am. Geophys. Union Trans., Vol. 27, No. 4, pp. 526-534.

Gustafsson, E., Klockars, C-E., 1981: Studies of groundwater transport in fractured crystalline rock under controlled conditions using non-radioactive tracers. Swedish Nuclear Fuel and Waste Management Co. SKBF/KBS Technical Report TR 81-07.

Hantush, M.S., Jacob, C.E., 1955: Non-steady radial flow in an infinite leaky aquifer. Am. Geophys. Union Trans., Vol. 36, pp. 95-100.

Källgården, J., Andersson, P., Holmqvist, M., 2002. History and current status on flow, pressure, water chemistry and installation at the TRUE-1 site. Äspö Hard Rock Laboratory International Progress Report IPR-02-46.

Moye, D.G., 1967: Diamond drilling for foundation exploration. Civil Eng. Trans., Inst. Eng. Australia (Apr. 1967), 95-100.

Nordqvist, R., 1994: Documentation of some analytical flow and transport models implemented for use with PAREST - Users manual. GEOSIGMA GRAP 94 006, Uppsala.

Ogata, A., Banks, R., 1961: A solution to the differential equation of longitudinal dispersion in porous media. U.S. Geol. Surv. Prof. Paper 411-A, Washington.

Svensk Kärnbränslehantering AB, 2001: First TRUE Stage - Transport of solutes in an interpreted single fracture. Proceedings from the 4th International Seminar Äspö, September 9-11, 2000. SKB TR-01-24. Swedish Nuclear Fuel and Waste Management Co.

Theis, C.V., 1935: The Relationship Between the Lowering of the Piezometric Surface and the Rate and Duration of Discharge Using Groundwater Storage. Trans. Am. Geophys. Union, Vol. 16, pp. 519-524.

Van Genuchten, M.Th., 1982: One-dimensional analytical transport modeling, in Proceedings: Symposium on unsaturated flow and transport modeling. Rep. PNL-SA-10325, Pacific Northwest Lab., Richland, Washington

Van Genuchten M.Th., Alves, W.J., 1982: Analytical solutions of the one-dimensional convective-dispersive solute transport equation. U.S. Dep. Agric. Tech. Bull. 1661.

Waterloo Hydrogeologic Inc. Aquifer Test version 2.0.

Winberg A. (ed), 1996: First TRUE Stage - Tracer Retention Understanding Experiments. Descriptive structural-hydraulic models on block and detailed scales of the TRUE-1 site. Swedish Nuclear Fuel and Waste Management Company. Äspö Hard Rock Laboratory International Cooperation Report ICR 96-04.

Winberg, A., Andersson, P., Hermanson, J., Byegård, J., Cvetkovic, V., Birgersson, L., 2000: Äspö Hard Rock Laboratory. Final report of the first stage of the Tracer Retention Understanding Experiments. SKB TR-00-07. Swedish Nuclear Fuel and Waste Management Co.

Zuber, A., 1974: Theoretical possibilities of the two-well pulse method. Isotope Techniques in Groundwater Hydrology 1974, Proc. Symp., Vienna 1974, IAEA,Vienna.

Appendix 1

Identification and location of packed-off borehole sections in the TRUE-1 array during the TRUE-1 Continuation tests CX-1 – CX-5. (C means sections equipped for tracer injection/sampling).

Borehole	Section	Borehole length (m)	Feature
KXTT1	R1	17.00 – 28.76	NW-2´
	R2	15.00 - 16.00 **C**	A
	R3	7.50 – 11.50 **C**	B
	R4	3.00 – 6.50	D
KXTT2	R1	16.55 – 18.30	A´
	R2	14.55-15.55 **C**	A
	R3	11.55 – 13.55 **C**	B
	R4	7.55-10.55	B
	R5	3.o5 -6.55	D
KXTT3	R1	15.42 – 17.43	NW-2´
	R2	12.42 – 14.42 **C**	A
	R3	8.92 – 11.42 **C**	B
	R4	3.17 – 7.92	B+D
KXTT4	S1	14.92 – 49.31	NW-2
	S2	12.92 – 13.92 **C**	A´
	S3	11.92 – 12.42 **C**	A
	S4	8.42 – 10.92	B
	S5	3.17 – 7.42	B+D
KXTT5	P1	10.81 – 25.85	NW-2
	P2	9.61 – 9.81	A
	P3	6.11 – 8.61	B
	P4	3.11 – 5.11	D
KA3005A	R1	51.03 – 58.11	?
	R2	46.78 – 50.03 **C**	B
	R3	44.78 – 45.78 **C**	A
	R4	39.03 – 43.78	A
	R5	6.53 – 38.03	A